Stiff and damage-tolerant metallic glasses

Von der Fakultät für Georessourcen und Materialtechnik der

Rheinisch-Westfälischen Technischen Hochschule Aachen

zur Erlangung des akademischen Grades eines

Doktors der Ingenieurwissenschaften

genehmigte Dissertation

vorgelegt von

Volker Schnabel, M.Sc.

aus Altenburg

Berichter: Univ.-Prof. Jochen M. Schneider, Ph.D.

Prof. Dr.-Ing. Dierk Raabe

Tag der mündlichen Prüfung: 09. Dezember 2015

Materials Chemistry Dissertation

No.: 25 (2015)

Volker Schnabel

Stiff and damage-tolerant metallic glasses

Shaker Verlag
Aachen 2015

Bibliographic information published by the Deutsche Nationalbibliothek
The Deutsche Nationalbibliothek lists this publication in the Deutsche Nationalbibliografie; detailed bibliographic data are available in the Internet at http://dnb.d-nb.de.

Zugl.: D 82 (Diss. RWTH Aachen University, 2015)

Printed in Germany.

ISBN 978-3-8440-4180-4
ISSN 1861-0595

Shaker Verlag GmbH • P.O. BOX 101818 • D-52018 Aachen
Phone: 0049/2407/9596-0 • Telefax: 0049/2407/9596-9
Internet: www.shaker.de • e-mail: info@shaker.de

Abstract

A paramount challenge in materials science is to design glasses that exhibit not only high strength but also toughness, i.e., the ability to resist brittle failure. This property combination constituting damage tolerance appears to be self-excluding; tough materials need to dissipate energy, for example, by plasticity, whereas high-strength materials are designed to prevent irreversible energy dissipation, thus plastic deformation[1]. Hence, materials exhibiting concomitant high toughness (where bond breakage occurs) and high strength (where bond breakage should not occur) are chimeric from the perspective of chemical bonding, imposing severe challenges on the design of these materials. Even though there are damage-tolerant glasses reported in literature[2], which are predominantly developed applying empirical alloying guidelines[3,4], the underlying physical and chemical mechanisms are not understood on the atomic scale. Hence, this work focuses on identifying the origin of damage-tolerant glasses. It has been reported in literature[5] that the elastic limit of metallic glasses exhibits a strong decrease with increasing temperature, which goes in hand with an increase in plastic deformation and hence an increase in toughness. To identify the origin of the temperature dependence of the plastic behaviour, *in situ* high-temperature X-ray diffraction experiments using high-energy photons and *ab initio* molecular dynamics simulations are performed to probe the temperature induced changes in topological short-range order in magnetron sputtered $Co_{67}B_{33}$ metallic glass thin films. Based on this correlative experimental and theoretical study the presence of B-Co-B rigid second order structures at room temperature and the temperature induced decrease in population of these strongly bonded building blocks is inferred. This notion is consistent with experimental reports[5] delineating the temperature dependence of elastic limit.

In addition to temperature, chemical composition is reported[6] to induce a change in brittle-ductile behaviour. Hence, within this work, *ab initio* molecular dynamics simulations are used to systematically explore the influence of alloying on the stiffness and plasticity of Co-Fe-Ta-B metallic glasses. The $Co_{43.5}Ta_{6.1}B_{50.4}$ metallic glass studied in this work, with a Young's modulus of 295 GPa, is the stiffest metallic glass known in literature. From the analysis of the density of the states it is suggested that the very large stiffness is due to strong covalent metal to B bonding. Furthermore it has been observed that by alloying with Y, Zr, Nb, Mo, Hf, W, C, N and O the Poisson's ratio can be varied from 0.293 to 0.342. As noted by Lewandowski *et al.*[3] a brittle-to-plastic transition for metallic glasses can be identified in the range of 0.31-0.32. The here observed increase in Poisson's ratio can be attributed to a change from predominately covalent to predominately metallic bond character. Thus, it can be perceived that the mechanical properties of metallic glasses are strongly affected by the interplay between chemistry and topology. However, up to now there is no high throughput method present in literature to study the chemically induced topological evolution of metallic glass thin films. Hence, a novel method is introduced which enables spatially resolved short range order analysis along concentration gradients of combinatorial metallic glass thin films. For this purpose a Co-Zr-Ta-B metallic glass thin film with a thickness of 3 µm is deposited on a thin polyimide foil, which is investigated by high energy X-ray diffraction in transmission mode. Through a correlative chemistry-topology-stiffness investigation along the Ta-B concentration gradient it is observed that an increase in metalloid concentration from 26.4 to 32.7 at.% and the associated formation of localized (hybridised) metal – metalloid bonds induce a 10 % increase in stiffness. Concomitantly, along the same composition gradient, a metalloid-concentration-induced increase in first order metal - metal bond distances of 1 % is observed,

which infers itinerant (metallic) bond weakening. Hence, the metalloid concentration induced increase in hybridised bonding dominates the corresponding weakening of metallic bonds. To evaluate the relevance of hybridisation for metallic glasses in general, the Poisson's ratio based design proposal of Lewandowski *et al.*[3] and Greaves *et al.*[4] is critically appraised. It is observed that data from this work, as well as results in the literature[4-6], are in conflict with the concept of Poisson's ratio serving as a universal parameter for fracture energy[4]. Here, the chemical origin of damage-tolerant glasses is identified at the electronic structure level. The correlative theoretical and experimental data reveal that the fraction of bonds stemming from deep core, hybridised states compared to the overall bonding defines damage tolerance in glasses. Consequently, Poisson's ratio alone is not sufficient to determine the brittle-ductile transition in glasses, and the contribution of hybridised states to the overall bonding defines the change from ductile to brittle behaviour.

Zusammenfassung

Eine zentrale Herausforderung in der Materialwissenschaft ist das Design von Gläsern, die nicht nur eine hohe Festigkeit sondern auch eine ausreichende Zähigkeit gegen Sprödbruch aufweisen. Diese Eigenschaftskombination aus Festigkeit und Zähigkeit, die auch als Schadenstoleranz bezeichnet wird, ist in sich Widersprüchlich. Während zähe Materialien bei Verformung Energie aufnehmen können, zum Beispiel durch Plastizität, sind hoch feste Materialien entwickelt, irreversible Energieaufnahme und somit plastische Verformung zu vermeiden[1]. Deshalb sind Materialien, die sowohl eine hohe Zähigkeit (Bindungen werden gebrochen) als auch eine hohe Festigkeit aufweisen (Bindungen sollten nicht gebrochen werden), aus der Perspektive des chemischen Bindungstyps widersprüchlich, was große Herausforderung für die Entwicklung solcher Materialien darstellt. Obwohl Berichte[2] von schadenstoleranten, metallischen Gläsern publiziert sind, wurden diese vorwiegend auf Basis von empirischen Legierungsrichtlinien[3,4] entwickelt ohne die zugrunde liegenden physikalischen und chemischen Mechanismen auf atomarer Ebene erfasst zu haben. Deshalb konzentriert sich diese Arbeit darauf den Ursprung schadenstoleranter Gläser zu identifizieren. Aus der Literatur[5] ist bekannt, dass die Fließgrenze von metallischen Gläsern eine starke Abnahme als Funktion der Temperatur aufweist, was mit einem Anstieg an Plastizität und somit Zähigkeit einhergeht. Um den Ursprung dieser Temperaturabhängigkeit zu verstehen werden *in situ,* Hochtemperaturbeugungsexperimente mit Hilfe von hochenergetischen Photonen und *ab initio* molekulardynamische Simulationen durchgeführt um die Temperatur induzierte Nahordnungsänderung von Dünnschicht $Co_{67}B_{33}$ metallischen Gläsern zu untersuchen. Basierend auf dieser korrelativen, experimentellen und theoretischen Studie wird die Präsenz von steifen B-Co-B

Strukturbausteinen zweiter Ordnung bei Raumtemperatur und die Temperatur induzierte Abnahme der Population von diesen Strukturbausteinen nachgewiesen. Diese Aussage ist konsistent mit experimentellen Arbeiten[5], die eine Temperatur induzierte Abnahme der Fließgrenze beschreiben. Wie in der Literatur[6] berichtet, kann zusätzlich zu der Temperatur auch eine Änderung der chemischen Zusammensetzung zu einem Übergang von sprödem zu plastischen Verhalten führen. Deshalb wird in dieser Arbeit auch der Einfluss von Legierungselementen auf die Steifigkeit und Plastizität von Co-Fe-Ta-B metallischen Gläsern systematisch mit Hilfe von *ab initio* molekulardynamischen Simulationen untersucht. Das hier simulierte $Co_{43.5}Ta_{6.1}B_{50.4}$ metallische Glas, weist mit einem E-Modul von 295 GPa die höchste in der Literatur beschriebene Steifigkeit eines metallischen Glases auf. Die Elektronendichteverteilung dieses Glases deutet darauf hin, dass die hohe Steifigkeit auf starke, kovalent gebundene Metall – Bor Bindungen zurück zu führen ist. In dieser Arbeit wird gezeigt, dass durch Legieren mit Y, Zr, Nb, Mo, Hf, W, C, N und O eine Poissonzahl zwischen 0.293 und 0.342 eingestellt werden kann. Wie von Lewandowski *et al.*[3] berichtet wurde, kann ein spröd-plastischer Übergang zwischen 0.31-0.32 identifiziert werden. Die hier beobachtete Anstieg der Poissonzahl kann auf eine Änderung von überwiegend kovalenten zu überwiegend metallischem Bindungscharakter zurückgeführt werden. Folglich sind die mechanischen Eigenschaften stark durch das Zusammenspiel von Chemie und Struktur bestimmt. In der Literatur wird keine effiziente Methode zur Untersuchung des Zusammenhangs von Chemie und Struktur bei metallischen Glasdünnschichten beschrieben. Aus diesem Grund wird hier eine neue Methode eingeführt, die die ortsaufgelöste Nahordnungsanalyse entlang eines Konzentrationsgradienten von kombinatorischen, metallischen Glasdünnschichten ermöglicht. Diese neue Methode bei der eine metallische Glasdünnschicht auf eine dünne Polyamidfolie aufgetragen

und mit hochenergetischer Röntgenbeugung im Durchstrahlverfahren untersucht wird, ermöglicht die hier durchgeführte Untersuchung einer kombinatorischen Co-Zr-Ta-B Glasdünnschicht. Mittels einer korrelativen chemischen-strukturellen-Steifigkeitsanalyse entlang des Ta-B Konzentrationsgradienten ist festzustellen, dass mit steigender Halbmetallkonzentration von 26.4 bis 32.7 at.%, und damit zusammenhängender Bildung von lokalisierten, hybridisierten Metall-Halbmetall Bindungen, ein Steifigkeitsanstieg von 10 % erreicht wird. Entlang desselben Konzentrationsgradienten wird ein Halbmetallkonzentration induzierter Anstieg der Metall-Metall Bindungsdistanz von 1 % beobachtet, woraus auf eine Abnahme der Metallbindungsstärke geschlossen werden kann. Somit dominiert der Halbmetallkonzentration induzierte Anstieg von hybridisierten Bindungen die einhergehende Abnahme der Metallbindungsstärke von Co-basierten metallischen Gläsern. Um die Relevanz der Hybridisierung für die Plastizität von metallischen Gläsern generell einschätzen zu können wird der Ansatz von Lewandowski *et al.*[3] and Greaves *et al.*[4] basierend auf dem Konzept der Poissonzahl kritisch begutachtet. Die Ergebnisse dieser Arbeit als auch Berichte aus der Literatur[4-6] stehen im Widerspruch mit dem Konzept, dass die Poissonzahl als universeller Parameter für die Bruchenergie dienen kann[4]. In dieser Arbeit wird der chemische Ursprung für schadenstolerante Gläser auf der Elektronenstrukturebene identifiziert. Aus den korrelativen, theoretischen und experimentellen Daten zeigt sich, dass der Anteil an Kern nahen, hybridisierten Bindungszuständen im Verhältnis zur Gesamtheit der Bindungszustände, die Schadenstoleranz von Gläsern definiert.

Folglich ist die Poissonzahl nicht ausreichend um den spröd-duktil Übergang von Gläsern zu beschreiben. Vielmehr definiert der Beitrag von hybridisierten Bindungszuständen im Verhältnis zu der Gesamtheit von Bindungszuständen den spröd-plastischen Übergang.

Preface

This work was supported by the Deutsche Forschungsgemeinschaft. The financial support within the SPP-1594 “Quantum mechanically guided design of ultra strong glasses” is gratefully acknowledged. This thesis is comprised of the following papers:

Paper I

Temperature Induced Short-Range Order Changes in $Co_{67}B_{33}$ Glassy Thin Films and Elastic Limit Implications

V. Schnabel, J. Bednarcik, D. Music, T. Pazur, C. Hostert, J. M. Schneider

Materials Research Letters 3 (2015) 82-87

Paper II

Stiffness and toughness prediction of Co-Fe-Ta-B metallic glasses, alloyed with Y, Zr, Nb, Mo, Hf, W, C, N and O by *ab initio* molecular dynamics

V. Schnabel, S. Evertz, H. Rueß, D. Music, J. M. Schneider

Journal of Physics: Condensed Matter 27 (2015) 105502

Paper III

Revealing the relationships between chemistry, topology and stiffness of ultrastrong Co-based metallic glass thin films: A combinatorial approach

V. Schnabel, M. Köhler, S. Evertz, J. Michalikova, J. Bednarcik,

D. Music, D. Raabe, J. M. Schneider

Under review

Paper IV

Damage-tolerant glasses defined by deep core electronic hybridisation

V. Schnabel, B. N. Jaya, M. Köhler, D. Music, C. Kirchlechner,

G. Dehm, D. Raabe, J. M. Schneider

In preparation

Other publications:

Paper V

Crystallization kinetics of V_2AlC

A. Abdulkadhim, M. to Baben, **V. Schnabel**, M. Hans, N. Thieme,
C. Polzer, P. Polcik, J.M. Schneider
Thin Solid Films 520 (2012) 1930

Paper VI

High temperature oxidation behaviour of Ti_2AlC ceramic at 1200°C

G.M. Song, **V. Schnabel**, C. Kwakernaak, S. van der Zwaag,
J.M. Schneider, W.G. Sloof
Materials at High Temperatures 29 (2012) 205

Paper VII

Bonding and elastic properties of amorphous $AlYB_{14}$

D. Music, F. Hensling, T. Pazur, J. Bednarcik, M. Hans,
V. Schnabel, C. Hostert, J.M.Schneider
Solid State Communications 169 (2013) 6

Paper VIII

On the effect of material processing: microstructural and magnetic properties of electrical steel sheets

S. Steentjes, D. Franck, K. Hameyer, S. Vogt, M. Benarz, W. Volk, J. Dierdorf,
G. Hirt, **V. Schnabel**, N.H. Marthuer, S. Korte-Kerzel
Electric Drivers Production Conference (2014) 1

Paper IX

Effect of Si additions on thermal stability and the phase transition sequence of sputtered amorphous alumina thin films

H. Bolvardi, M. to Baben, F. Nahif, D. Music, **V. Schnabel**, K. P. Shaha, S. Mraz, J. Bednarcik, J. Michalikova, and J. M. Schneider
Journal of Applied Physics 117 (2015) 025302

Paper I: V. Schnabel synthesised the thin films, performed the chemical characterisation and the molecular dynamics simulations. J. Bednarcik did the reciprocal space analysis. The real space analysis and further topological analysis was done by V. Schnabel. T. Pazur with assistance of C. Hostert and V. Schnabel developed the “Atomic structure analysis package” for the analysis and visualization of the molecular dynamics simulation data.

Paper II: The molecular dynamics simulations were done by V. Schnabel, with the assistance of S. Evertz and H. Rueß. Topological and density of states analysis was done by V. Schnabel.

Paper III: The synthesis and topological analysis was done by V. Schnabel. The atom probe tomography analysis was done by M. Köhler. The chemical and stiffness measurements along the concentration gradient were done by S. Evertz.

Paper IV: V. Schnabel synthesised the glasses and performed the molecular dynamics simulations. B.N. Jaya, M. Köhler and C. Kirchlechner carried out the mechanical experiments and characterized the glasses.

For all papers, goals were discussed and strategies were developed with J.M. Schneider. D. Music guided the molecular dynamics simulations. All co-authors took part in discussion of the results and writing the manuscripts.

Danksagung

An erster Stelle danke ich Prof. Jochen M. Schneider. Durch deine Gabe Sachverhalte offene, ehrliche und präzise auf den Punkt zu bringen hast Du mich schon zu Studentenzeiten beeindruckt. Ich bin dankbar und mit Stolz erfüllt, dass Du mir die Chance geboten hast am Lehrstuhl für Werkstoffchemie zu promovieren und glücklich über Alles, was ich von Dir lernen durfte.

Denis, ich möchte Dir sehr herzlich für deinen Rat, die tollen Gespräche und insbesondere deiner munteren Art danken.

Meiner Ansicht nach ist die große Stärke des MCh der Zusammenhalt des Lehrstuhls. Ich danke meinen Kollegen für die Unterstützung und die tolle Zeit am Lehrstuhl für Werkstoffchemie. Während meiner Promotion war es mir immer eine Freude mit unserer Administration, unseren Werkstätten und allen sogenannten „nicht Wissenschaftlern“ zusammen zu arbeiten. Für die sehr interessante, effiziente und erfüllende Zusammenarbeit möchte ich mich bei Euch bedanken.

Von ganzen Herzen danke ich Susanne. Danke für deine Liebe, deine Geduld und deine Unterstützung.

Ich danke meiner Familie, meiner Schwester Silke, meiner Mutter Margit und meinem Vater Harald dafür, dass Ihr immer für mich da seid, wenn man euch braucht. Liebe und Zeit sind zwei der teuersten Güter der Welt, von denen Ihr mir schon so viel geschenkt habt. Eure Unterstützung hat mich stets begleitet und mich mit Stärke und Mut erfüllt. Dafür danke ich Euch.

Table of contents

1 Introduction

Metallic glasses are amorphous solids with a high degree of topological and chemical short range order[7] which exhibit fascinating structural and functional properties[8]. For example Co-Fe-Ta-B based bulk metallic glasses have an extremely high maximum permeability of 500,000 and very low coercivity[8] of 0.26 A/m. Due to such excellent soft magnetic properties Co,Fe-based bulk metallic glasses show great potential for consolidated magnetic cores for power supply applications[9]. Also, Inoue *et al*. report with > 5000 MPa a very large elastic limit[5]. The combination of the high elastic limit and the smooth surface render these metallic glasses suitable for micro components e.g. micro gears for high precision endoscopes[8,10], spring microactuators[11] and micro electro-mechanical systems devices[12]. However, it has been observed that Co-based metallic glasses exhibit brittle behaviour at room temperature[5], whereas other e.g. Pd-based[2] or Zr-based[13] systems exhibit large plastic deformations upon fracturing, which is essential for tough behaviour. The combination of both high strength and toughness appears to be self-excluding from the chemical bond perspective. Tough materials are designed to exhibit large plastic deformation, whereas high strength materials, exhibiting large elastic limits are designed to prevent plastic deformation. This inverse bond character imposes challenges on the design of these materials. Yet, the property combination of both high strength and toughness, constituting damage tolerance[2] is very attractive for applications[8,10,12]. However, for metallic glasses the underlying physical and chemical principles constituting damage tolerance are not identified. It is the main goal of this work to identify the origin of damage-tolerant glasses at the electronic structure level. Hence, it is of key importance to apprehend the chemically induced brittle-tough transition in metallic glasses. Furthermore, it has been reported that the brittle-tough transition in Co-based metallic glasses is also induced by increasing temperature[5]. Before

addressing the main goal the temperature induced topological changes, as well as the chemical induced stiffness and plasticity changes are investigated.

1.1 Damage tolerance

Damage tolerance, as well as production costs, stiffness, weight, wear rate, thermal expansion, electrical and thermal conductivity are possible criteria for materials design[14]. Furthermore, layout, application and economic boundary conditions determine the relevance of these criteria for commercial products. In the case of damage tolerance the application also defines, which materials properties constitute damage tolerance. To illustrate the dependence of damage tolerance on the application, the materials selection processes for a pressure vessel and a micro gear are discussed.

For a pressure vessel the most devastating failure is brittle fracture induced bursting[14]. Hence, pressure vessels are designed to either leak or yield before brittle fracture. Brittle failure is induced for crack lengths exceeding stable crack growth, which is determined by the material fracture toughness[15] (K_{IC}). At a constant pristine crack length and defined pressure, the fracture toughness of a pressure vessel material should be as high as possible to assure tough behaviour. Furthermore, the "yield before break" criterion[14] implies that the chosen material should exhibit a high tendency towards yielding or in other words a low elastic limit (σ_f). Hence, in the case of pressure vessel materials damage tolerance constitutes a combination of high toughness and low elastic limit. By considering this combination a materials selection parameter $C1$ (Eq. 1.1) can be defined, which needs to be large for the selection of damage-tolerant pressure vessel materials.

$$C1 = \frac{K_{IC}}{\sigma_f}$$

Equation 1.1

A materials selection guideline with a constant value of 0.1 $m^{0.5}$ for $C1$ is depicted in Fig. 1.1, where the fracture toughness is presented as a function of the elastic limit for polymers, foams, silica glasses, technical ceramics, Ti-alloys, Al-alloys, steels, SiON thin films and conventional metallic glasses[12,14,16].

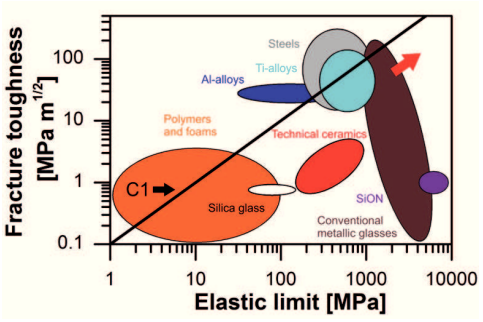

Figure 1.1: The fracture toughness is presented as a function of the elastic limit for polymers and foams, silica glasses, technical ceramics, Ti-alloys, Al-alloys, steels, SiON thin films and conventional metallic glasses[12,14,16]. The black line indexed with $C1$ represents the chosen selection guideline for damage-tolerant pressure vessel materials.

Every material above the selection guideline indicated by $C1$ e.g. some polymers, some Al-alloys, some Ti-alloys, some steels and some high toughness metallic glasses meet the defined damage tolerance criterion. However, as described by Eq. 1.2, for a spherical pressure vessel with a thin wall the pressure p, radius R and wall thickness t correlate to the stress σ in the vessel wall[14].

$$\sigma = \frac{pR}{2t}$$

Equation 1.2

In case the ratio of pressure, radius and thickness is exceeding the elastic limit, the pressure vessel material starts to yield, which is not intended under stable operation. As an example polypropylene[14] (PP) with σ_f = 29 MPa, stainless steel[14] with σ_f = 400 MPa and $Pd_{79}Ag_{3.5}P_6Si_{9.5}Ge_2$ bulk metallic glass, which is considered to be a benchmark glass in terms of damage tolerance[2], with σ_f = 1500 MPa are compared as pressure vessel materials. By applying Eq. 1.2 on a defined working pressure of 200 bar and a vessel radius of 1 m the wall thickness of the vessel should be larger than 345, 25 and 7 mm for PP, stainless steel and metallic glass, respectively, in order for the vessel not to yield under operation. In Table 1.1 the elastic limit, fracture toughness, the ratio of fracture toughness to elastic limit C and the calculated minimum wall thickness are summarized for PP, stainless steel and the metallic glass, respectively. All three materials exhibit fracture toughness to elastic limit ratios larger than the defined selection guideline of $C1$ equal to 0.1 $m^{0.5}$. Even though the applied Eq. 1.2 is an analytical description for pressure vessels with thin walls, the comparison shows that vessels under high pressure made out of polymers are not practical even though the requirements regarding damage tolerance are met, whereas stainless steel and metallic glass may still be feasible solutions considering the above defined damage tolerance selection guideline. Hence, next to the damage tolerance at least one more design criterion, of a maximum wall thickness should be defined. Furthermore, it can be learned from the materials comparison that high strength metallic glasses are outstanding materials when size matters. This conclusion is also reflected in the second example, namely micro gears for endoscopes.

Next to optical systems, endoscopes can contain instrumentation e.g. clamps, tweezers or slings for the execution of surgical actions[17]. Today's endoscopic

surgeries are capable of inflicting minimal trauma upon a patient[17], which is due to the continuous size decrease of endoscopes (Fig. 1.2a)[8,17].

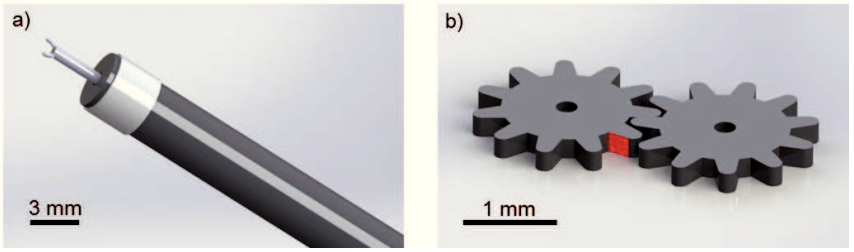

Figure 1.2: a) Schematic drawing of an endoscope equipped with a micro clamp (adopted from[17]). b) Schematic drawing of micro gears with a diameter[8] of 1.5 mm.

As the size of the endoscope decreases the mechanical parts e.g. gears decrease in size as well, whereas the average force to clamp a vein stays unchanged. Hence, the load acting on the face of the gear's tooth, which is coloured in red in Fig. 1.2b is maintained. However, for decreasing gear sizes also the tooth size and the tooth face area decreases. Though, a maintained load acting on a decreasing area implies increasing stress, which for gear diameters below 3 mm leads to stresses exceeding the elastic limit of metallic materials e.g. steels[18]. Due to plastic deformation of the teeth, micro steel gears exhibit a low durability in acceleration tests of micro gear motors[18]. In contrast high strength metallic glass gears with GPa elastic limits[5,8] exhibit a 313 times higher durability[18].

However, next to plastic deformation, brittle fracture of the micro components should be prevented[5,8]. For the prevention of brittle failure also a high toughness is required. Consequently, in the case of micro gears damage tolerance is constituted by the combination of high strength and toughness. Hence, as presented in Table 1.1 only the metallic glass exhibits the required combination of both high strength and toughness.

Material	σ_f MPa	K_{IC} MPa·m$^{0.5}$	C m$^{0.5}$	t mm	Suitable vessel material	Suitable micro gear material
Polypropylene	29	3.8	0.13	345	not practical (high t)	no (low σ_f)
Stainless steel	400	150	0.38	25	yes	no (low σ_f)
$Pd_{79}Ag_{3.5}P_6Si_{9.5}Ge_2$	1500	200	0.13	7	yes	yes

Table 1.1: Summary of the elastic limit σ_f, fracture toughness K_{IC}, the ratio of fracture toughness to elastic limit C and the calculated minimum wall thickness t for polypropylene, stainless steel and the $Pd_{79}Ag_{3.5}P_6Si_{9.5}Ge_2$ metallic glass, respectively[14]. Furthermore, the summary of the materials selection process is presented.

One could also expand the term damage tolerance to e.g. wear and thermal behaviour, which leads to the conclusion that the application determines the term damage tolerance. However, since high strength and high toughness appear from the bond character as mutually exclusive materials properties, imposing severe challenges on the design of these materials, this work concentrates on damage-tolerant glasses, which combine high strength and toughness, indicated by the red arrow in Fig. 1.1. Furthermore, the material strength is evaluated by the elastic limit.

1.2 Current alloying guidelines

According to Lewandowski *et al.*[3] the bulk modulus B to shear modulus G ratio is an indication for a transition from brittle to plastic behaviour. Equivalently, Rouxel *et al.*[19] have proposed Poisson's ratio ν (Eq. 1.3) to relate to the packing density and network dimensionality of glasses and hence serves as a universal parameter for fracture energy[4]. However, Poisson's ratio by definition describes only elastic behaviour; for materials with a small Poisson's ratio and hence a small bulk-to-shear

modulus ratio, a pressure-induced elastic volume change is favoured over a shape change by shear. On the other hand, materials exhibiting a large Poisson's ratio resist a volume change in favour of a shape change by shear.

$$\nu = \frac{3\,B/G - 2}{6\,B/G + 2}$$

Equation 1.3

In literature the Poisson's ratio is proposed as an alloying guideline for tough glasses[4], which is inferred to be due to the correlation between topology, toughness and Poisson's ratio. Greaves *et al.*[4] propose that cross-linked structures oppose both elastic transverse contraction, which is reflected in Poisson's ratio and plastic deformation, being essential for high toughness. As a transition range a Poisson's ratio of 0.31-0.32 from brittle to plastic behaviour is proposed for metallic glasses. Similar observations are made by Pugh[20], who studied the transition from brittle to plastic behaviour of crystalline phases as a function of their B/G ratio. Pugh identified for cubic close-packed (ccp) metals a lower transition range with a Poisson's ratio ranging from 0.26-0.31[20]. Hence, it can be concluded that the mechanisms that govern plastic deformation in metallic glasses may be different from metals. Furthermore, the necessary Poisson's ratio to govern plastic deformation in metallic glasses needs to be larger compared to ccp metals.

Even though the mechanisms that are proposed in literature to govern plasticity in metallic glasses e.g. shear transformation zones[21] may be complex, Poisson's ratio as a simple criterion based on elastic constants seems to predict the tendency towards plastic behaviour well for some metallic glasses[3]. However, data from this work as well as results in the literature[4-6], are in conflict with the concept of Poisson's ratio serving as a universal parameter for fracture energy[4]. By unravelling the

chemical origin of the transition from brittle to tough behaviour at the electronic structure level, this work enables knowledge-based design of novel damage-tolerant metallic glasses using *ab initio* predictions while explaining previous reports of deviation from expected behaviour.

2 Methods

2.1 Theoretical methods

The time-independent Schrödinger equation (Eq. 2.1) describes the quantum behaviour of atoms,

$$\left[-\frac{\hbar^2}{2m} \sum_{i=1}^{N} \nabla_i^2 + \sum_{i=1}^{N} V(\mathbf{r}_i) + \sum_{i=1}^{N} \sum_{j<1} U(\mathbf{r}_i \mathbf{r}_j) \right] \psi = \mathcal{E}\psi$$

Equation 2.1

where m denotes the electron mass, $\hbar$ denotes Planck's constant, N denotes the number of electrons, ψ denotes the electron wave function, $\mathcal{E}$ is the ground state energy of the electrons and the three terms within the brackets denote the kinetic energy of each electron, the interaction energy between each electron and the collection of atomic nuclei, and the interaction energy between different electrons, respectively[22]. Hence, Schrödinger's equation for a solid material is a many-body problem. The complexity of this problem can significantly be decreased by density functional theory (DFT), which rests on the Hohenberg-Kohen theorem[23] that the ground-state energy is a unique functional of the electron density $n(\mathbf{r})$,

$$\mathcal{E} = \mathcal{E}\,[n(\mathbf{r})]$$

Equation 2.2

and that the electron density, which minimizes the energy of this functional is the electron density fully solving Schrödinger's equation[22]. A reasonable description of the Hohenberg-Kohen theorem is expressed in Eq. 2.3,

$$\mathcal{E}[\{\psi_i\}] = \mathcal{E}_{\text{known}}[\{\psi_i\}] + \mathcal{E}_{\text{XC}}[\{\psi_i\}]$$

Equation 2.3

where the $\mathcal{E}_{\text{known}}$ term includes the electron kinetic energies, the Coulomb interactions between the electrons and the nuclei, the coulomb interactions between pairs of electrons, and the Coulomb interactions between pairs of nuclei, whereas the exchange-correlation functional $\mathcal{E}_{\text{xc}}$ includes all the quantum mechanical effects that are not included in the first term[22]. Commonly used approximations for the exchange-correlation function are the local density approximation (LDA) and the generalized gradient approximation (GGA), or more distinctively the Perdew-Wang functional (GGA PW91)[24], which is used within this work[22]. Furthermore a 3x3x3 Monkhorst-Pack grid[25] for reciprocal-space integration, an energy cut-off of 500 eV and a convergence criterion of 0.01 meV was applied for the ground state calculations.

Within this thesis two codes based on DFT were employed. *Ab initio* molecular dynamics (MD) simulations were conducted using the Open source package for Materials Explorer (OpenMX)[26] code, version 3.7. The calculations at 0 K were performed using the Vienna Atomic Simulation Package (VASP), version 5.2.12[27]. OpenMX was used for the molecular dynamic simulations, because it has an advantage regarding computational speed compared to VASP.

For the MD simulations electronic potentials with the generalized gradient approximation and basis functions in the form of linear combination of localized pseudoatomic orbitals were applied[28,29]. The following basis functions were used Co5.5-s2p1d1, Fe5.0-s1p2d1, Ta7.0-s2p1d1f1, B4.5-s2p2, Y6.5-s3p2d1, Zr7.0-s2p1d1, Nb7.0-s2p1d1, Mo6.0-s2p1d1, Hf6.0-s2p1d1f1, W6.0-s2p1d1f1, C4.5-s2p1, N4.5-s2p1, O4.5-s2p1, Pd5.0-s2p1d1, Al6.0-s2p2 and Cu4.5-s1p1d13. Here the first symbol denotes the chemical name, followed by the cutoff radius and

the set of primitive orbitals applied. An N-point grid larger than 72x72x72 and a cutoff energy of 150 Ry was used.

To assure a realistic representation of the short-range order within the *ab initio* molecular dynamic simulations the method[30] previously validated by Hostert *et al.* for Co-Fe-Ta-B[30] and Co-Fe-Ta-Si[31] was applied as schematically depicted in Fig. 2.1.

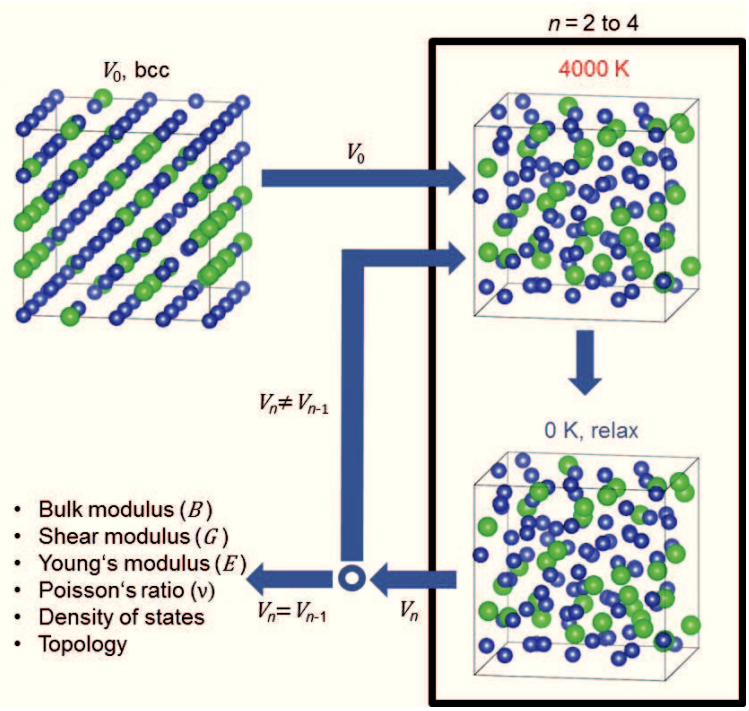

Figure 2.1: Schematic representation of the *ab intio* molecular dynamics simulation method applied.

The initial configuration of the atoms was a bcc super cell with 128 lattice sites containing 115 atoms and 13 vacancies. An amorphous structure was obtained by performing *ab initio* MD simulations, through heating the cell to 4000 K by scaling the velocity for 400 fs. A step size of 1 fs was applied. Afterwards the structure was

quenched with an infinite quenching rate to 0 K and relaxed in terms of atomic positions and volume.

Using the amorphous, stress free structure the cell was heated up to 4000 K again for 400 fs to enable a stress free diffusion. The process of heating the amorphous structure at 4000 K and calculating the stress free volume at 0 K was performed two to four times until the volume after the last heating and the second to last heating converge within 2 %.

The elastic properties, the electron density distributions and the topological information were obtained at 0 K from the stress free configurations after the last heating cycle. For the ground state calculations spin-polarization was taken into account, whereas it was neglected within the MD simulations of the melt. The bulk modulus was obtained using the Birch-Murnaghan equation of state[32]. The shear modulus according to Hill[33] was calculated from the elastic constants C_{11}, C_{12} and C_{44}, which were obtained by distorting the cubic symmetry and fitting with a second-order polynomial function[34]. The Poisson's ratio and Young's modulus E was obtained from the shear and bulk moduli[33].

The pair distribution functions[30] (PDF) $g(r)$ of the structurally relaxed systems were obtained from the atomic positions of the individual species within the simulation by applying Eq. 2.4,

$$g(r)=\frac{1}{4\pi\rho_0 r^2}\sum_i\sum_j\frac{b_i b_j}{\langle b\rangle^2}\delta(r-r_{ij})$$

Equation 2.4

where the sum goes over all pairs of atoms i and j within the model system separated by r_{ij}. In order to be able to compare to experimental work, the X-ray scattering power was taken into account. The b_i denotes the scattering power of atom i and $\langle b\rangle$ is the

average scattering power of the model. The average atomic number density and atomic distance is denoted by ρ_0 and r, respectively.

For the investigation of the temperature induced topological evolution of the $Co_{67}B_{33}$ system the super cell from the last heating cycle was quenched to 2000 K and held at this temperature for 1000 fs. Thereafter, a stepwise structure analysis was performed. The temperature step size was chosen to be 100 K and the time held at each step was 500 fs. This yields in an approximate cooling rate of $2 \cdot 10^{14}$ K/s. For the structural analysis the last 250 fs of each temperature step was taken into account. The MD time step was set to 1 fs. The topological evolution was examined by calculating total and partial pair distribution functions, bond angle distribution and Voronoi tesselation.

Based on Voronoi tessellation the atom specific nearest neighbor coordination was estimated[35] by utilizing the atomic coordinates of the relaxed *ab initio* MD data as input, defining the configuration for each temperature. In this work, the radical plane method was applied, which takes the atomic radii of the atoms into account[36]. When projected planes meet, edges are formed and consequently faces of polyhedra. These polyhedra are described by the Voronoi index $[n_3, n_4, n_5, n_6]$, where n_i denotes the number of i-edged faces of the Voronoi polyhedron. For the analysis and visualization of OpenMX data the “Atomic structure analysis package”[37] was used.

2.2 Experimental methods

2.2.1 Magnetron sputtering

Metallic glass thin films were synthesised by magnetron sputtering, using the ultra-high vacuum system schematically depicted in Fig. 2.2 with a base pressure lower than $6 \cdot 10^{-5}$ Pa. Elemental targets, with a diameter of 50 mm were used. For the metallic targets separate direct current power supplies and for the B target radio frequency power supplies were utilized. The elemental targets had a purity larger than 99.9 % and 99.5 % for the metals and B, respectively. During deposition the argon partial pressure was 0.4 Pa. The target to substrate distance was 10 cm.

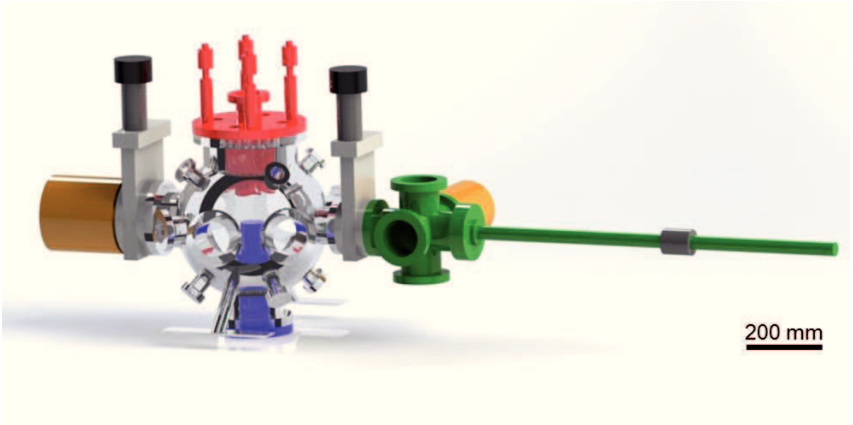

Figure 2.2: Schematic drawing of the ultra-high vacuum sputtering system used. The magnetron cluster flange, substrate holder, load lock system and turbo pumps are depicted in red, blue, green and orange, respectively.

For the investigation of the temperature induced topological evolution of the $Co_{67}B_{33}$ metallic glass, homogeneous thin films were deposited using substrate rotation with 30 rpm. The target power densities were set to be 1.6 $W \cdot cm^{-2}$ for Co and 8.4 $W \cdot cm^{-2}$

for B. The deposition time was 6 hours, resulting in a film thickness of 3 µm. As a substrate, polycrystalline sodium chloride was used, which was later removed from the metallic glass thin film by rinsing it with demineralized water, acetone and methanol. The so obtained powder was later examined by energy dispersive X-ray analysis (EDX) and high energy X-ray diffraction (XRD).

For the investigation of the chemistry-topology-mechanical property relationship along a composition gradient of Co-Zr-Ta-B metallic glass thin films, combinatorial films were magnetron sputtered onto Si and polyimide substrates. The film deposited onto the 50.8 mm Si (100) substrate was used for chemical and mechanical characterization, while the films on 50 µm thick radiation damage tolerant polyimide foil[38] were employed for structural analysis. The base pressure[39] of the system was $6 \cdot 10^{-5}$ Pa. The films were synthesised from circular elemental targets with a diameter of 50 mm and a purity of 99.95 % for Co, Zr and Ta and 99.5 % for B. The applied power densities were 2.0, 1.6, 0.3 and 8.4 W/cm^2 for Co, Zr, Ta and B targets, respectively. The three metals were sputtered using separate direct current (DC) power supplies, whereas B was sputtered with a radio frequency power supply. As a sputtering gas Ar with a pressure of 0.4 Pa was employed. The targets were tilted by 19° normal to the substrate as described in Fig. 2.3 and the target to substrate distance was 10 cm. The deposition time was 3 hours resulting in a film thickness of 3 µm. A spacing between the individual measuring points of 4 mm was chosen, corresponding to a gradient of 0.2 at.% B per mm along the Ta-B gradient.

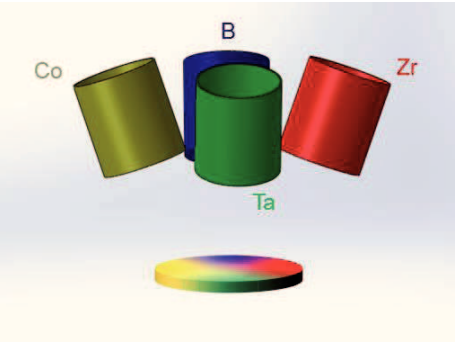

Figure 2.3: Schematic drawing of the combinatorial deposition setup. The chemical symbols denote the direction of the elemental sputtering sources, which results in the schematic compositional gradient depicted. The measurements were performed along the B – Ta and the Co – Zr gradient with a spacing of 4 mm between the individual measurement points.

For the micro-fracture experiments homogeneous $Pd_{57.0}Al_{23.9}Cu_{11.4}Y_{7.7}$, $Co_{42.0}Fe_{13.2}Zr_{10.7}Ta_{6.6}B_{27.5}$, $Co_{58.4}Fe_{7.0}B_{34.6}$, $Cu_{67.8}Zr_{32.2}$ and $Co_{68.3}Zr_{31.7}$ metallic glass thin films were synthesised. As substrate material single crystal (001) Si wafer were used.

2.2.2 Chemical characterisation

The chemical composition and purity of the $Co_{67}B_{33}$ thin film powder was analysed by standard less EDX analysis at an acceleration voltage of 4 kV using a JEOL, JSM-6480 scanning electron microscope equipped with an detector from EDAX performing a background, atomic number, absorption and fluorescence correction. All other EDX measurements were performed with the same equipment at an acceleration voltage of 16 kV using atom probe tomography (APT) measurements as a standard. 3D-APT samples of the metallic glass thin films were prepared using a focused ion beam (FIB) (FEI Helios Nanolab 600i dual-beam FIB) equipped with a micromanipulator.

The APT tips were prepared according to a standard lift-out procedure[40], and final shaping was performed with low energy (5 keV) to prevent Ga implantation. The APT measurements were performed on a commercial local electrode atom probe (LEAP 3000X HR, CAMECA Instruments) in voltage mode at a base temperature of 60 K, 200 kHz pulse repetition rate, 15% pulse fraction and 1% target evaporation rate. The acquired datasets were analysed using the reconstruction software IVAS 3.6.8[41] (CAMECA Instruments). In particular, frequency distribution analysis[28,29] was used to determine the homogeneity of the compositions (block size 100 atoms).

2.2.3 Topological characterisation

The topology analysis was performed applying high energy X-ray diffraction at the P02.1 beamline of the PETRA III electron storage ring at DESY (Hamburg, Germany). For the *in situ* investigation of the $Co_{67}B_{33}$ metallic glass thin film high-energy, high-temperature XRD experiments were performed in transmission geometry using a Linkam THMS 600 heating stage. The separated metallic glass thin film sample was put into a quartz capillary with a wall thickness of 20 µm and a diameter of 1 mm. The sample was heated from room temperature up to 863 K at a heating rate of 10 K/min. Heating was done under protective Ar atmosphere. The sample was instantaneously illuminated with a monochromatic photon beam (wavelength λ=0.02073 nm). Diffracted photons were recorded with a fast image plate detector Perkin Elmer 1621. Two-dimensional XRD patterns were acquired every 12 s. The sample to detector distance was set to 32.3 cm. Due to heater geometry the maximum wave vector q ($q=4\pi \sin\theta/\lambda$) was limited to 14 $Å^{-1}$. The topological anaylsis along the concentration gradient of the Co-Zr-Ta-B thin films was done in transmission with a beam size of 0.7x0.7 mm using the thin film sample deposited on polyimide foil. Each measuring point was illuminated for 30 s. The

sample to detector distance was set to be 24.6 cm, whereas the *q* vector up to 14 $Å^{-1}$ was used[42].

Two-dimensional XRD patterns were integrated to the *q*-space using the software package FIT2D[43]. The data were then converted to the total structure factor, *S(q),* using standard procedures described elsewhere[30,44]. The integrated data were corrected for sample absorption, fluorescence contribution and inelastic (Compton) scattering. The total structural factor *S(q)* was obtained from the normalized elastically scattered intensity. The pair distribution functions were obtained from the structure factor through a sine Fourier transform using standard procedures described elsewhere[30].

2.2.4 Mechanical characterisation

To obtain the reduced Young's modulus a depth-sensing nanoindenter (Hysitron TriboIndenterTM) was utilized. A Berkovich indenter with a tip radius of 100 nm was used. The maximum load was set to correspond to a contact depth of less than 10 % of the film thickness. 24 indentations were performed for each film composition. The Oliver and Pharr method[39] was applied to extract the reduced Young's modulus.

For the micro-fracture experiments the Si substrate was etched out using 30% KOH solution at 70°C to obtain free-standing thin films of the sputtered metallic glasses. Focused ion-beam (FEI Helios Nanolab 600i dual-beam FIB) milling was used to prepare the micro-cantilevers. Coarse cuts were made at 2.5 nA (30 kV), and final polishing was performed at 80 pA (30 kV) to obtain cantilevers of approximately 18 µm × 2.5 µm × 2.5 µm. The cantilevers for fracture toughness measurements were pre-notched at a lower current of 7.7 pA (30 kV). Both the notched and un-notched specimens were loaded *in situ* into the scanning electron microscope (JEOL-JSM 2000) using the ASMEC UNAT-2 indenter. A conical tip (1 µm tip radius) was

used to load all microbeams in displacement control at a constant rate of 5 nm/s. The loading sequence involved numerous loads/unloads over multiple cycles. The pop-in/fracture load corresponding to the crack propagation event in the notched beams was used as input in the analytical formula for determination of K_{Ic} from either linear elastic fracture mechanics (LEFM) for the brittle glasses or from J-integral measurements for the ductile metallic glasses. The testing technique and analysis follows the procedure established by Matoy *et al.*[16] and Wurster *et al.*[45] for K_{Ic} and J_{Ic} determination, respectively. The fracture toughness of the $Co_{68.3}Zr_{31.7}$ thin films was also calculated using extended finite element simulations of the cantilever bending in Abaqus 10.1 to cross-check the validity of the results from the analytical formula. The fracture load of the unnotched beams was used to determine[16] the maximum bending (yield/fracture) strength σ_c. A total of 80 samples were tested, with 8 un-notched and 8 notched beams for each composition. The beams were imaged both before and after fracture to follow the crack trajectory. The strain energy release rate (fracture energy) (G_c) is obtained from Eq. 2.5[46] using either the K_{Ic} or J_{Ic} values for all metallic glass thin films.

$$G_c = J_{Ic} = \frac{K_{Ic}^2(1-\nu^2)}{E}$$

Equation 2.5

3 Results and discussion

3.1 Temperature induced topological evolution of $Co_{67}B_{33}$

Co,Fe-based bulk metallic glasses show a strong temperature dependent elastic limit from the ultra-high strength of 5185 MPa at room temperature to 1100 MPa at 873 K, while the elastic modulus of 268 GPa appears to be preserved[5]. It is proposed in literature that deformation within the super cooled liquid state the apparent viscosity is sample size dependent, due to confinement of collective shear events[47]. The very high stiffness of these metallic glasses at room temperature is according to Wang *et al.*[48] and Hostert *et al.*[30] caused by the presence of strong, covalent Co-B and (Co,Fe)-B bonds, respectively.

Since temperature induced changes in topology and/or chemical ordering have not been investigated by theoretical or by experimental means the underlying cause of the strong temperature dependence of the elastic limit in Co,Fe-based bulk metallic glasses is unknown. The objective of this work is to identify the temperature induced topological evolution of the $Co_{67}B_{33}$ metallic glass thin films, to enable knowledge based design of new metallic glasses with high strength and plasticity at room temperature. To this end *in situ* high temperature, high-energy X-ray diffraction experiments[49] in combination with *ab initio* molecular dynamics simulations[30] is employed.

3.1.1 Experiments

The temperature induced topology evolution is initially examined by comparing the PDFs obtained from *in situ* high-energy, high-temperature XRD experiments with the PDFs simulated with *ab initio* MD. Fig. 3.1 shows series of the structure factors of the $Co_{67}B_{33}$ powder as a function of temperature in a three dimensional plot at the top

and a colour intensity plot at the bottom. A common feature for the structure factors below 758 K is that they exhibit broad principal peak located at 3.21 $Å^{-1}$ followed by rather broad peaks of rapidly decaying intensity towards larger q-values. This is a fingerprint of missing long range order in the material studied and confirms its fully amorphous nature. However, the number as well as the intensity of the individual structure factor peaks drastically increase at 758 K as crystallization of the $Co_{67}B_{33}$ metallic glass powder sets in. The structure of the crystallized material is consistent with the stoichiometric Co_2B phase (JCPDS 25-0241). Hence, the onset of crystallization for $Co_{67}B_{33}$ is at 758 K, which is lower than the crystallization temperatures of quaternary Co-Fe-Ta-B bulk metallic glasses, which have been reported to be in the range of 940-980 K[5,50]. This is expected as it is known that for binary systems as compared to systems with a larger number of components the number of possible local atomic configurations is lower leading to a decrease in glass stability[9].

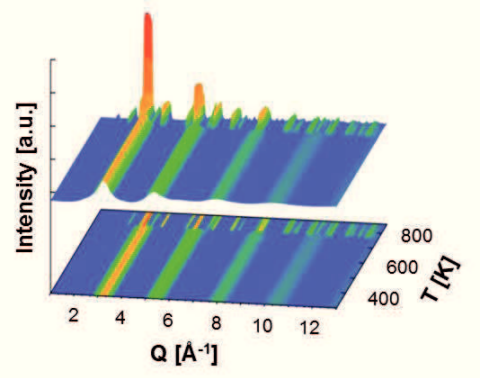

Figure 3.1: Structure factor of $Co_{67}B_{33}$ as a function of temperature (T) measured by *in situ* high temperature XRD.

In Fig. 3.2 the PDFs obtained by XRD experiments and MD simulations at selected temperatures are shown. All the PDFs discussed describe the order prior to crystallization (see Fig. 3.1). Comparing the experimental PDFs with the ones obtained by MD simulation one can see that all main features, such as the peaks' heights and their positions, are in very good agreement. Hence, the computational methodology based on Hostert *et al.*[30] and Music *et al.*[37] appears to be useful to describe the temperature dependent topology of Co-B metallic glass thin films. In Fig. 3.2 the first structural peak at 1.98 Å corresponds to the first coordination shell of Co-B interatomic bond length distribution, which is learned from the partial PDFs obtained by *ab initio* MD (see Fig. 3.3). The second peak at 2.55 Å corresponds to the first Co-Co coordination shell. The amplitude of Co-Co bond length distribution is higher compared to Co-B bond length distribution, which is due to the larger weighting factor of Co compared to B. Furthermore, there are no distinct features of B-B bonds visible in the total PDFs shown in Fig. 3.2. Peaks at distances larger than 2.55 Å can be attributed to the second and third coordination shells. The position of the first bond length distribution maxima does not change by increasing the temperature from 300 to 700 K. The bond length distribution of the second coordination shell is characterized by two, equally temperature independent maxima at 4 and 5 Å, which according to van de Waal[51] may imply some spatial orientation coherence between the first and second coordination shell as well as the presence of dense tetrahedral packing[52].

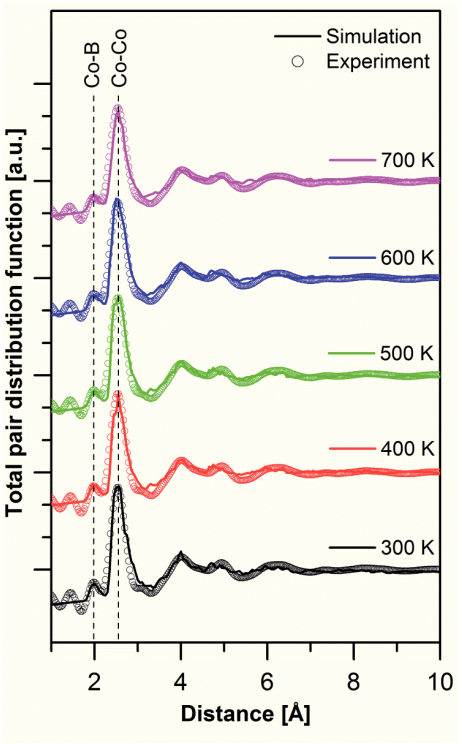

Figure 3.2: Comparison between the *in situ* measured and *ab intio* molecular dynamics, total pair distribution data in the temperature range of 300 to 700 K. For better comparison curves are vertically offset.

From the investigation of the structure factors and the total pair distribution functions very good agreement between theory and experiment is observed. However no cause of the experimentally observed temperature dependent mechanical behaviour could be identified as all total PDFs, which are dominated by Co-Co interactions appear to be temperature independent.

To probe the temperature induced changes in structure further the partial PDFs obtained by *ab initio* MD simulation shown in Fig. 3.3 are examined. In an attempt to

overcome the limitations posed by the extensive simulation time requirements during *ab initio* MD simulations[53], the analysis of partial PDFs obtained at temperatures exceeding the experimentally studied temperature range is performed.

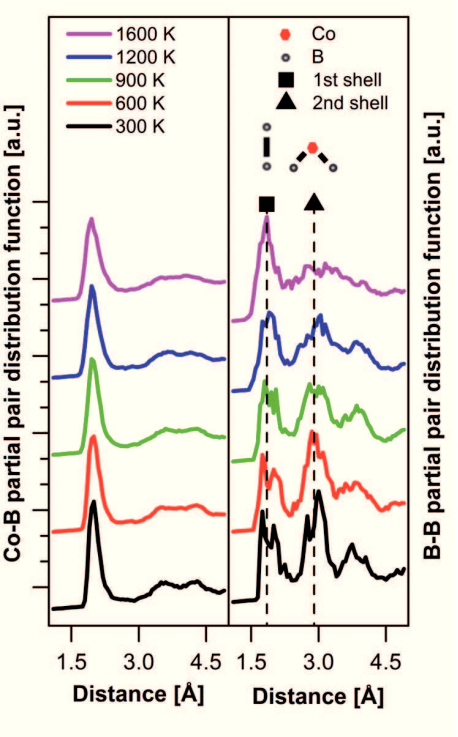

Figure 3.3: The atomic Co-B (left panel) and B-B (right panel) partial pair distribution function data obtained by *ab inito* molecular dynamics simulation in the temperature range of 300 to 1600 K are shown. The vertical lines correspond to the square and the triangular symbol indicates the location of the first and second B-B coordination shell, respectively.

On the left side of Fig. 3.3 the partial Co-B PDFs are shown in a temperature range of 300 to 1600 K. For the partial PDFs the *r*-range shown is 1 to 5 Å. The first peak at

1.98 Å corresponds to the first coordination shell of Co-B pairs. With a deviation of 1 % such bond length is in good agreement with the Co-B bond distance as observed in case of the quaternary Co-Fe-Ta-B metallic glass[30]. With increasing temperature the peak broadens and its amplitude decreases, which is due to a wider distribution of Co-B bond lengths. At 300 and 600 K the second peak and the third peak corresponding to the second coordination shell of Co-B bond length exhibit maxima at 3.5 and 4.3 Å, respectively. The two peaks broaden and finally merge as the temperature is increased, which can be explained by the loss of coherence between the first and second Co-B coordination shell[51].

On the right side of Fig. 3.3 the B-B partial PDFs from the temperature range of 300 to 1600 K are shown. At room temperature there are three peaks visible, whereas at 1600 K the B-B partial PDF is dominated by the first peak as the second and the third peak have merged to a broad peak which is strongly reduced in amplitude. The first B-B coordination shell, which corresponds to the first peak at 1.85 Å is indicated by squares. The distance of the second B-B coordination shell (indicated by triangles) is 2.9 Å. At room temperature the second B-B coordination shell shows a higher amplitude than the peak of the first coordination shell. This observation is consistent with other B containing metallic glass systems[52,54]. It is evident that the partial distribution functions of both B-B and Co-B are strongly affected by temperature. However, at this point it is unclear which building blocks can be associated with the decrease in bond length distribution amplitude that has been observed as the temperature is increased.

To determine which building block(s) can be associated with the second B-B peak, the angular distribution of the B-Co-B structure is examined. On the left side of Fig. 3.4 the angular distribution of B-Co-B bonds in the temperature range of 300 to 1600 K is shown. For all temperatures there are three peaks visible at 55°, 90° and

140°. The peak at 90° shows the largest fraction of B-Co-B bond angles for all temperatures. However, the peak at 90° broadens indicating a population density decrease as the temperature is increased. From the partial PDFs shown in Fig. 3.3 one can learn that the first Co-B shell distance is equal to 1.98 Å at 300 K. B-Co-B structures with a Co-B distance of 1.98 Å and a bond angle of 90°, result in B-B distance of 2.82 Å. This value is in very good agreement with the second coordination shell distance obtained in the calculation of the B-B partial distribution function shown in Fig. 3.3. Therefore, it is evident from the correlative analysis of the partial distribution functions and the bond angle distribution data that the population of B-Co-B building blocks with a 90° bond angle that are present at room temperature is drastically reduced as the temperature is increased. It is reasonable to assume that this temperature induced decrease in population of covalently bonded[30,48], and therefore stiff B-Co-B building blocks has implications for the mechanical properties: As mentioned above the elastic limit of Co-based metallic glasses shows a strong temperature dependence[5]. According to Inoue *et al.*[5] the elastic limit of $Co_{43}Fe_{20}Ta_{5.5}B_{31.5}$ drops by 80 % as the temperature is increased from room temperature to 873 K. The temperature dependence of the elastic limit is consistent with the temperature induced loss of coherence between the first and second Co-B coordination shell and the temperature induced decrease in population of stiff B-Co-B building blocks, which is inferred from the partial PDFs and the B-Co-B bond angle analysis. Even though there is a difference in absolute temperature between the experimentally observed drop in elastic limit[5] and the observed loss of coherence between the first and second Co-B coordination, the inferred topology evolution provides insight towards designing high strength (Co,Fe)-based metallic glasses. This difference may be due to the different chemistry, sample size or limitations posed by the extensive simulation time requirements towards relaxation.

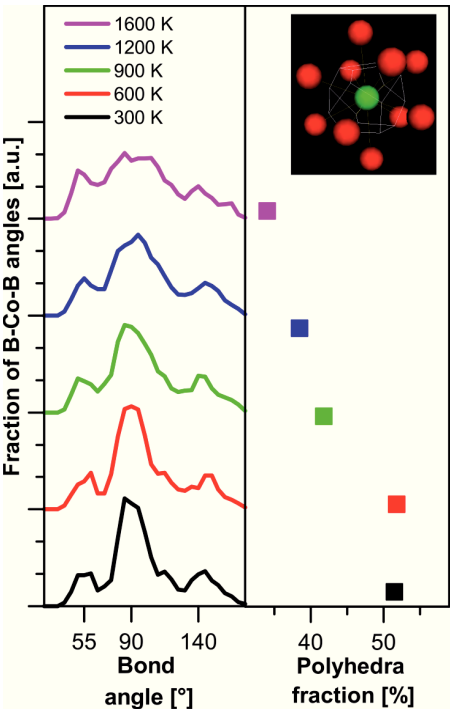

Figure 3.4: The bond angle distribution of the B-Co-B bonds in the temperature range of 300 to 1600 K obtained by *ab inito* molecular dynamics simulation is shown (left panel). The fraction of Frank-Kasper like Voronoi polyhedra is shown in the same temperature range (right panel). Furthermore, an example of the most dominant B centred bicapped square Archimedean antiprism, with the Voronoi index of (0,2,8,0) is given in the upper right corner.

It is proposed by Zhang *et al.*[55] that plastic behaviour is promoted by decreasing the fraction of Frank-Kasper like polyhedra. With a decrease in fraction of densely packed polyhedra the fraction of ready to flow region increases, which on the one hand promotes plastic behaviour and on the other hand decreases the chance for severe shear localization[55]. An increase of ready to flow regions may cause a change

in deformation mode from shear band dominated mode to homogeneous deformation mode as it is seen for many metallic glasses[5,56,57]. On the right side of Fig. 3.4 the fraction of densely packed Co and B centred Frank-Kasper like Voronoi polyhedra is shown in the temperature range of 300 to 1600 K. The most dominant polyhedron at 300 K is the B centred bicapped square Archimedean antiprism (Fig. 3.4), with the Voronoi index of (0,2,8,0). Hence, the B centred short range order present in the crystalline phase is also present in the glass structure. In contrast to the crystalline phase, in which every B atom has the same short range order only 12 % of the B centred polyhedra in the glass have that particular coordination. The fraction of densely packed Frank-Kasper like Co and B centred polyhedra decreases from 50 % at 300 K to about 35 % at 1600 K. This implies a significant increase in fraction of ready to flow regions as the temperature is increased[55], which is consistent with the experimentally observed drop in elastic limit[5]. The temperature induced decrease in population of Frank-Kasper like polyhedra is also consistent with above presented notion on the temperature induced loss of coherence between the first and second Co-B coordination shell and the structural changes derived by the partial PDFs.

A key issue in designing ductile metallic glasses is controlling shear band nucleation and propagation[58]. The here reported temperature induced changes in topological and chemical order cause an increase in the population of ready to flow regions, which facilitates ductile behaviour[5]. Future materials design strategies may focus on decreasing structural coherence between the first and second coordination shell, by alloying to stabilize ready to flow regions at lower temperatures.

3.2 *Ab initio* stiffness and toughness prediction

In addition to temperature depend plastic behaviour, also composition depended brittle-ductile transitions are reported[3,4]. *Ab inito* calulations have been proven to be well suited for calculation of elastic constants[59-61]. Furthermore, Hostert *et al.*[30,31] have observed good agreement between experiment and *ab initio* molecular dynamics simulation of Co-based metallic glasses, regarding topology, correlations between electronic structure, elasticity, density and magnetism. Therefore it is shown that *ab initio* MD simulations are suitable to do knowledge based design of Co-based metallic glasses. Large experimental effort is needed in order to evaluate the plasticity of metallic glasses[12,62,63] and the existing alloy strategies are based on heuristic principles[64]. The present MD simulation studies from literature are either on the origin of deformation mechanisms[65] or evaluate only a narrow range of composition[55]. For Co-B based metallic glasses the Co-Ta-B[48], the Co-Fe-Ta-B[30] and the Co-Fe-Ta-Si system[31] have been individually investigated by MD simulation.

However, up to now there is no systematic quantum mechanically guided materials design study available on the influence of substantial chemical composition variations on the stiffness and plasticity of Co-based metallic glasses. The goal of this work is to understand the influence of chemical composition on the stiffness and plasticity of Co-based metallic glasses by systematically alloying and investigating the electronic fingerprint responsible for plastic or stiff behaviour. In literature the metal to metalloid interaction has been identified to be of key importance for the mechanical properties of these type of high stiffness metallic glasses[66,67]. The initial selection of alloying candidates is based on the work of Hostert *et al.*[30], who identified strong, covalent (Co, Fe)-B bonds to cause the high stiffness of Co-Fe-Ta-B metallic glasses. In order to affect the covalent nature of the metal to B bond, the first computational strategy

focuses on systematically varying the valence electron concentration and size by substituting Fe with transition metals namely Y, Zr, Nb, Mo, Hf and W. The second computational strategy focuses on systematically investigating the metal to non-metal interactions by substituting B with other non-metals namely C, N and O. The third computational strategy focuses on the influence of non-metal concentration by increase the B content up to 50 at.% by substituting Fe.

3.2.1 Molecular dynamics simulations

The change in Young's modulus, which is a measure for stiffness, is shown in Fig. 3.5 as a function of chemical composition for the transition metal alloying strategy. For each transition metal there are 6.1 and 9.6 at.% of Fe replaced by Y, Zr, Nb, Mo, Hf and W, respectively. To study the influence of low alloying concentrations there is a third simulation performed for 1.7 at.% of Nb. The intercept of the horizontal line with the vertical axis at 273 GPa represents the Young's modulus of $Co_{43}Fe_{20}Ta_{5.5}B_{31.5}$ obtained by Hostert *et al.*[30] by *ab initio* MD simulation. This line represents the benchmark in terms of stiffness for metallic glasses in general and is included as a guide for the eye.

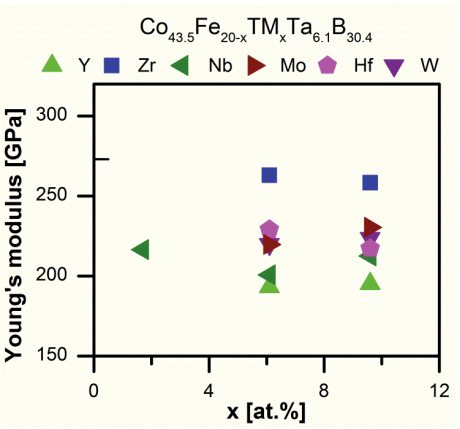

Figure 3.5: The Young's modulus obtained by *ab initio* calculations for $Co_{43.5}Fe_{20-x}TM_xTa_{6.1}B_{30.4}$ as a function of chemical composition x in at.%, where TM stands for Y, Zr, Nb, Mo, Hf and W respectively. The intercept of the horizontal line with the vertical axis at 273 GPa represents the Young's modulus of $Co_{43}Fe_{20}Ta_{5.5}B_{31.5}$ obtained by *ab initio* MD simulation[30] .

All the Young's modulus values presented in Fig. 3.5 are lower than the reference value of $Co_{43}Fe_{20}Ta_{5.5}B_{31.5}$. The highest Young's modulus of 263 GPa is calculated for $Co_{43.5}Fe_{13.9}Zr_{6.1}Ta_{6.1}B_{30.4}$. The lowest value of 193 GPa is calculated for $Co_{43.5}Fe_{13.9}Y_{6.1}Ta_{6.1}B_{30.4}$. It can be observed that the stiffness decreases, as the Zr and Hf content is increased from 6.1 to 9.6 at.%. On the other hand for W, Mo, Y and Nb the stiffness increases, as the content is increased from 6.1 to 9.6 at.%. In the case of Nb alloying the calculation of 6.1 at.% is showing a minimum and the stiffness increases towards the low content of 1.7 at.%. What can be learned from the results of the first computational alloying series is that the Young's modulus can be varied in the range of 193 to 263 GPa. However to maximize the stiffness, Fe should not be replaced by the metals examined in this work, for all compositions examined within the transition metal alloying strategy yield lower stiffness compared to the

quaternary $Co_{43}Fe_{20}Ta_{5.5}B_{31.5}$ studied by Hostert *et al.*[30]. Hence, varying the valence electron concentration by alloying with the transition metals Y, Zr, Nb, Mo, Hf and W does not increase the stiffness of the $Co_{43}Fe_{20}Ta_{5.5}B_{31.5}$ metallic glass system.

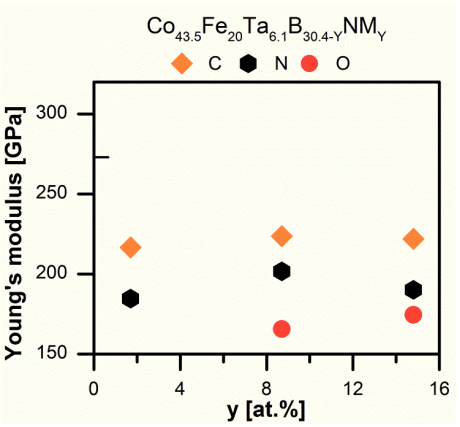

Figure 3.6: The Young's modulus obtained by *ab initio* calculations for $Co_{43.5}Fe_{20}Ta_{6.1}B_{30.4-y}NM_y$ as a function of chemical composition y in at.%, where NM stands for C, N and O, respectively. The intercept of the horizontal line with the vertical axis at 273 GPa represents the Young's modulus of $Co_{43}Fe_{20}Ta_{5.5}B_{31.5}$ obtained by *ab initio* MD simulation[30].

The effect on the Young's modulus for the non-metal alloying strategy is shown in Fig. 3.6. In this case up to half of B is replaced by either C, N or O. For all three elements there are simulations performed for 8.7 and 14.8 at.%. In addition there are simulations performed for low C and N contents of 1.7 at.%. Also in Fig. 3.6 the reference of $Co_{43}Fe_{20}Ta_{5.5}B_{31.5}$ is shown[5,30].

Within the non-metal alloying strategy, the carbon containing systems exhibit the highest Young's modulus, which varies only slightly with C content between 217 and 224 GPa. The second highest Young's modulus values are observed for the N containing systems in a range of 185 to 202 GPa. In this case a maximum for the N

content of 8.7 at.% is observed. The lowest stiffness is observed if B is replaced with O, which leads to Young's modulus values of 166 and 174 GPa. From Fig. 3.6 it can be seen that in the case that B is replaced by C, N or O the Young's modulus is reduced by more than 30 GPa. Therefore, it can be concluded that lowering the B content in the $Co_{43}Fe_{20}Ta_{5.5}B_{31.5}$ system leads to a decrease in Young's modulus. This observation is consistent with the proposal of Hostert *et al.*[30] that strong covalent (Co,Fe)-B bonds are responsible for the high stiffness of this group of metallic glasses. In the case that the population of metal to B bonds is responsible for the high stiffness of these type of metallic glasses, an increase in B content should lead to more of these stiff structures and thereby leading to a higher Young's modulus. In order to study the influence of increased B content the third alloying strategy mentioned above is employed.

In order to investigate the influence of increased non-metal concentration on the stiffness of the $Co_{43}Fe_{20}Ta_{5.5}B_{31.5}$ system the Fe concentration is decreased from 20 to 10.4 and 0 at %, by replacing Fe with B. In Fig. 3.7 the calculated Young's modulus is shown as a function of increasing B content. The calculated Young's modulus for the $Co_{43.5}Fe_{10.4}Ta_{6.1}B_{40}$ system is 256 GPa, whereas the Young's modulus of the $Co_{43.5}Ta_{6.1}B_{50.4}$ system is 295 GPa, which is 8 % higher compared to the reference $Co_{43}Fe_{20}Ta_{5.5}B_{31.5}$ metallic glass[30]. Hence, the $Co_{43.5}Ta_{6.1}B_{50.4}$ metallic glass composition calculated here yields the highest stiffness ever reported for a metallic glass. For knowledge based design of metallic glasses with a high Young's modulus it is important to identify the origin of the high stiffness of the $Co_{43.5}Ta_{6.1}B_{50.4}$ metallic glass.

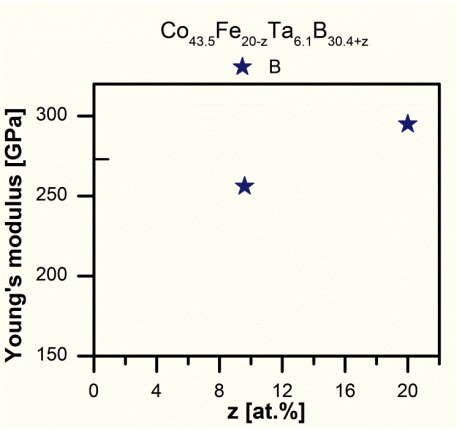

Figure 3.7: The Young's modulus obtained by *ab initio* calculations for $Co_{43.5}Fe_{20-z}Ta_{6.1}B_{30.4+z}$ as a function of chemical composition z in at.%. The intercept of the horizontal line with the vertical axis at 273 GPa represents the Young's modulus of $Co_{43}Fe_{20}Ta_{5.5}B_{31.5}$ obtained by *ab initio* MD simulation[30].

As already mentioned above the very high stiffness of the Co-based metallic glasses at room temperature is according to Wang *et al.*[48] and Hostert *et al.*[30] caused by the presence of strong, covalent Co-B and (Co,Fe)-B bonds, respectively. Hence, in order to identify the cause for the large variations in Young's modulus the total and partial density of states for the very stiff $Co_{43.5}Ta_{6.1}B_{50.4}$ system and the low stiffness $Co_{43.5}Fe_{20}Ta_{6.1}B_{15.8}O_{14.8}$ system are investigated. The total and partial density of states for the $Co_{43.5}Ta_{6.1}B_{50.4}$ system are shown on the left side of Fig. 3.8. The magnetic moment for Co present in this system is with up to 1.04 μ_B very low, therefore no distinction between spin up and spin down states are presented. It is observed that even with the high B content the overall bonding character is metallic since the Fermi level is occupied. The most dominating region in the total density of states is from 0 to -5 eV. Furthermore, all three elements are contributing considerably to the total density of states. The largest contribution to the density of

states for Co, Ta and B originates from the 3d, 5d and 2p orbitals, respectively. The most dominating region for all partial density of states is from -2.5 to -5 eV. Furthermore there are deep core states occupied for Co and B at -10 eV. In the most dominating region from -2.5 to -5 eV, strong hybridisation between all three species is observed, indicating strong covalent metal to B bonding. It is proposed that the strong hybridisation in the region of -2.5 to -5 eV and the strong hybridisation in the deep core states at -10 eV cause the extraordinary high stiffness of the $Co_{43.5}Ta_{6.1}B_{50.4}$ system.

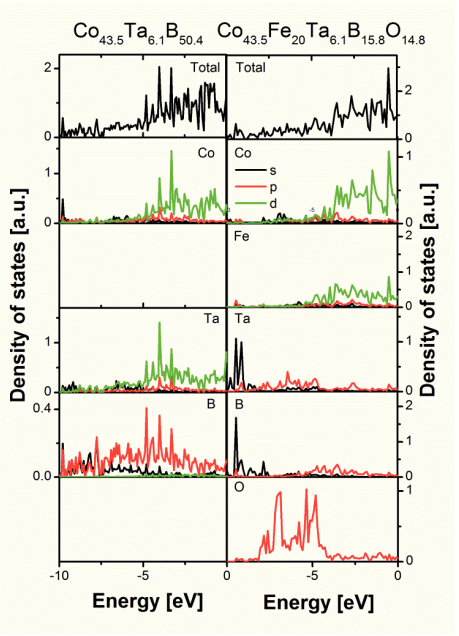

Figure 3.8: The total and partial density of states for the $Co_{43.5}Ta_{6.1}B_{50.4}$ system is shown on the left. The Fermi level is set to 0 eV. The total and partial density of states for the $Co_{43.5}Fe_{20}Ta_{6.1}B_{15.8}O_{14.8}$ system is shown on the right.

The total and partial density of states for the $Co_{43.5}Fe_{20}Ta_{6.1}B_{15.8}O_{14.8}$ system are shown on the right side of in Fig. 3.8. Comparing the total density of states of the two systems studied, one can see that the peaks of the $Co_{43.5}Fe_{20}Ta_{6.1}B_{15.8}O_{14.8}$ system are shifted to higher energies. This is a first indication for the weaker bonding nature. Also with the oxygen content of 14.8 at.% the Fermi level is occupied and the overall bonding character is metallic. The magnetic moments for the $Co_{43.5}Fe_{20}Ta_{6.1}B_{15.8}O_{14.8}$ system are 2.11 and up to 1.63 μ_B for Fe and Co, respectively. As for the $Co_{43.5}Ta_{6.1}B_{50.4}$ system no distinction between spin up and spin down is presented. It can be seen that the total density of states are dominated by the partial Co and Fe density of states, where Co and Fe partial density of states show a similar behaviour. Therefore it can be concluded that Co and Fe are similar in their bonding behaviour within this system. The most dominating region for the Co partial density of states is between -2.5 and 0 eV, which is closer to the Fermi level compared to the $Co_{43.5}Ta_{6.1}B_{50.4}$ system. In contrast to the $Co_{43.5}Ta_{6.1}B_{50.4}$ system the Ta 5d orbitals are less occupied in the $Co_{43.5}Fe_{20}Ta_{6.1}B_{15.8}O_{14.8}$ system and the Ta 6s orbitals are occupied at an energy of about -10 eV. For B the most dominating region is also at about -10 eV, where the 2s orbitals are occupied. For O the 2p orbitals are pronounced, which are mainly occupied between -5 and -7.5 eV. As mentioned above the total density of states is dominated by the partial Co and Fe density of states. Hence, the contributions of Ta, B and O to the overall bonding are small. Furthermore there is less hybridisation in the $Co_{43.5}Fe_{20}Ta_{6.1}B_{15.8}O_{14.8}$ system compared to $Co_{43.5}Ta_{6.1}B_{50.4}$ system. The difference in hybridisation in the energy range of -2.5 to -5 eV and the shift of the total density of states closer to the Fermi level are proposed to be the cause for the low stiffness of the oxygen containing systems studied in this work. Hence, the observations made within this work are

consistent with literature, where the strong covalent metal to B bonding[30,48] is proposed to cause the high stiffness of Co-based metallic glasses.

In order to correlate the electronic structure with the present topology, PDFs for the stiff $Co_{43.5}Ta_{6.1}B_{50.4}$ system and the low stiffness $Co_{43.5}Fe_{20}Ta_{6.1}B_{15.8}O_{14.8}$ system are presented in Fig. 3.9. In the upper part of Fig. 3.9 the PDF for the $Co_{43.5}Fe_{20}Ta_{6.1}B_{15.8}O_{14.8}$ system is presented, whereas in the lower part the PDF for the $Co_{43.5}Ta_{6.1}B_{50.4}$ system is presented. For both systems the presented distance is between 1.5 and 8.5 Å. In both systems there can be three short range order features observed. For the $Co_{43.5}Ta_{6.1}B_{50.4}$ system the first feature at a bond distance of 1.75 Å can be attributed to first order B-B bonding. The second feature at 2.05 Å can be attributed to first order metal to B bonding and the third feature at 2.55 Å, which has the highest amplitude, can be attributed to first order metal to metal bonding. The amplitude of the first and second feature is lower compared to the third metal – metal feature, due to the low weighting factor[68] of B. The bond distances observed are in good agreement to literature[30,66,69]. Comparing the amplitude of the metal to non-metal bond population of the $Co_{43.5}Ta_{6.1}B_{50.4}$ and the $Co_{43.5}Fe_{20}Ta_{6.1}B_{15.8}O_{14.8}$ system it can be observed that the metal to non-metal population of the $Co_{43.5}Ta_{6.1}B_{50.4}$ system is higher. It is reasonable to assume that a higher population of the covalently bonded metal to non-metal bonds leads to the observed increase in stiffness, which is consistent with the density of states analysis. Hence, through the correlative electronic structure and topology analysis it can be inferred that the $Co_{43.5}Ta_{6.1}B_{50.4}$ system exhibits a large population of strongly bonded metal to non-metal bonds, which leads to the high Young's modulus of 295 GPa.

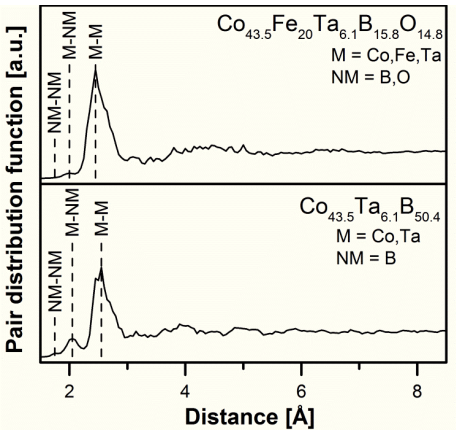

Figure 3.9: The pair distribution function for the $Co_{43.5}Fe_{20}Ta_{6.1}B_{15.8}O_{14.8}$ and the $Co_{43.5}Ta_{6.1}B_{50.4}$ system.

For many highly loaded micro components a material is demanded, which exhibits next to a high stiffness also moderately ductile behaviour[8]. Therefore, a plasticity design strategy based on *ab initio* calculations is proposed: It has been observed experimentally by Inoue *et al.*[5] that $Co_{43}Fe_{20}Ta_{5.5}B_{31.5}$ shows brittle behaviour at room temperature. This quaternary metallic glass has a Poisson's ratio of 0.283[30]. Hence, the observed brittle behaviour is consistent with the notion of Lewandowski *et al.*[3], who observed a threshold range of 0.31 to 0.32 for a transition from brittle to plastic behaviour. Metallic glasses with a Poisson's ratio lower than this range have a tendency to show brittle behaviour and metallic glasses with Poisson's ratios higher than this range are observed to show plastic behaviour with energy release rates[3] of up to 100 kJ/m. In order to predict the tendency towards plastic behaviour of the alloy compositions studied in this work the Poisson's ratio is calculated. The Young's modulus as a function of Poisson's ratio for all alloy compositions is shown in Fig. 3.10. The shaded region is indicating the reported transition range from brittle

behaviour on the left, towards plastic behaviour on the right[3]. With a Poisson's ratio of 0.283[30] the $Co_{43}Fe_{20}Ta_{5.5}B_{31.5}$ metallic glass is exhibiting brittle behaviour. The same holds for the very stiff $Co_{43.5}Ta_{6.1}B_{50.4}$ metallic glass system and the two compositions containing Zr. However, most of the other systems studied in this work exhibit Poission's ratios larger than the threshold region, and therefore more homogeneous deformation behaviour is expected, which infers more plasticity[55]. From Fig. 3.10 one can learn that the Poisson's ratio exhibits compositional induced changes from 0.293 to 0.342. This allows for designing the plastic behaviour by alloying. Substitution of B with N or O leads to a large Poission's ratio and the substitution of Fe with Nb, W and Mo also leads to Poisson's ratios above the critical threshold. It can also be seen from Fig. 3.10 that with increasing Poisson's ratio, which is an indication for a tendency towards plastic behaviour, the Young's modulus is decreasing. From the density of states evaluation above, it can be learned that the very stiff $Co_{43.5}Ta_{6.1}B_{50.4}$ system shows a high degree of hybridisation and therewith strong covalent metal to B bonds, which may also explain the tendency towards brittle behaviour. On the other hand the density of states for the $Co_{43.5}Fe_{20}Ta_{6.1}B_{15.8}O_{14.8}$ system is dominated by the partial density of states of Co and Fe. Furthermore, the degree of hybridisation is lower, which indicates a metallically dominated bonding character. Hence this may explain the tendency towards plastic behaviour, which is consistent with the high Poisson's ratio of 0.340.

As it can been seen from Lewandowski's work[3] the energy release rate increases logarithmically with increasing Poisson's ratio above the threshold range. Hence, for some applications it can be desirable to design for plastic behaviour by alloying even if this means compromising the ultrahigh stiffness.

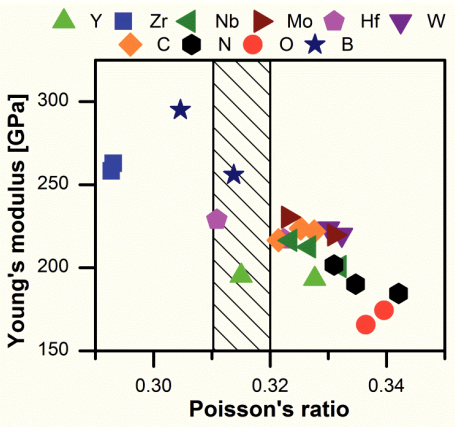

Figure 3.10: The Young's modulus obtained by *ab initio* calculations as a function of Poisson's ratio for all systems studied in this work. The shaded region is indicating the transition range from brittle behaviour on the left, towards plastic behaviour on the right, which was proposed by Lewandowski *et al.*[3].

3.3 Chemistry, topology and stiffness relationship

It can be perceived from the work presented so far that both chemistry and topology strongly affect the mechanical properties of Co-based metallic glasses. Also in literature the chemistry-topology-property relationships of metallic glasses have been a topic of intense discussion[68,70-73]. Metallic glasses fall into two groups, namely those with[67] and those without metalloids[74]. The most common synthesis techniques for metallic glasses are bulk casting[75-77] and melt spinning[78]. In these studies, chemical composition is varied through multiple synthesis experiments. By employing conventional bulk synthesis techniques, metallic glasses are developed as a result of multiple, sequential bulk synthesis experiments, often based on trial-and-error approaches[5,68,70,79-81]. In contrast, combinatorial thin film synthesis has been used to systematically study the chemistry-topology-property relationship of various material systems[60,82]. Recently, combinatorial metallic glass synthesis by physical vapour deposition has been employed to study the chemistry – mechanical property relationship of metallic glass thin films[83]. Furthermore, literature has shown clear agreement between bulk and thin film properties of Co-based metal-metalloid metallic glasses regarding elasticity, density and magnetism[30,31]. Ergo, combinatorial thin film synthesis can be an efficient tool to investigate the chemistry-topology-property relationship of metallic glasses in general. However, up to now there is no high throughput method present in literature to study the chemically induced topological evolution along a defined compositional gradient of metallic glass thin films[83]. The short range order of metallic glasses is usually studied by sequential synthesis of homogeneous specimen and analysis employing high energy diffraction experiments[30,31,70,73], which is an inefficient way of investigating the chemistry-topology-mechanical properties relationship.

The topology of metallic glasses without metalloids is strongly determined by dense packing[55,74], whereas the topology of metal-metalloid metallic glasses is additionally influenced by strong covalent bonding[30,48,67,73]. Due to the complex chemistry-topology-property relationships the design of metal-metalloid metallic glasses is challenging[5,67,84]. The metal-metalloid Co-based metallic glasses discussed here possess a unique local atomic configuration[48,69,73], which leads to the combination of extraordinary high fracture strength of 5185 MPa and high Young's modulus of 268 GPa[5]. It is inferred in the literature that through chemically induced topology changes, properties such as glass formability[67,70,71], magnetic properties[68] and mechanical properties[30,71,72,85] can be enhanced. The Young's modulus[30,48] as well as the elastic limit[73] have also been reported to exhibit a strong topological dependence. In the case of Co-based metallic glasses it has been observed that the metal-metalloid short range order is strongly affecting the mechanical properties[30,31,48,73]. Furthermore, it has been reported for Fe-Cr-Mo-P-C-B metallic glasses that an increase in metalloid concentration increases the number of strongly bound metal-metalloid clusters, which on the other hand weakens the metal-to-metal bonds[67]. These chemical-induced topology changes have implications on how shear stress may be accommodated[67]. Hence, an influence on the Young's modulus, shear modulus and plasticity of these type of metal-metalloid metallic glasses has been observed[67]. The discussion above suggests that understanding the chemistry-topology-property relationship is an essential prerequisite to the knowledge-based design of strong metallic glasses.

The objective of this work is to describe the chemically induced topology and stiffness changes of Co-Zr-Ta-B metallic glass thin films. A novel method is introduced, where the chemically induced topology and stiffness changes are measured along a composition gradient of Co-Zr-Ta-B metallic glass thin films. For this purpose a

combinatorial metal-metalloid Co-Zr-Ta-B metallic glass thin film is deposited by physical vapour deposition[30,86] on low X-ray scattering and radiation damage tolerant thin polyimide foil[38]. The topological analysis of the combinatorial thin film is performed in transmission, using high energy X-ray diffraction[42].

3.3.1 Experiments

Chemical analysis

Due to the geometrical arrangement of the magnetrons with respect to the substrate normal (Fig. 2.3) and the chosen 10 cm target to substrate distance, the deposition of the chemically graded thin films is achieved. The Co content obtained by the combinatorial deposition ranges from 31.9 to 45.5 at %, the Zr content from 26.1 to 34.4 at %, the B content from 26.4 to 32.7 at %, and the Ta content from 1.0 to 2.6 at %. The magnitude of the composition gradients are a consequence of the power supplied to the magnetrons and the difference in sputter yield of the elements[87].

Short range order analysis

Four representative pair distribution functions obtained from measurements along the B-Ta concentration gradient are presented in Fig. 3.11 in a range of 2 to 4 Å. The PDFs are presented with an equally spaced offset in vertical direction for better comparison purposes. The dashed lines in Fig. 3.11 represent the total PDFs, whereas the solid and dotted graphs represent Gaussian deconvolutions of two individual bond population distributions. It can be observed that for all compositions the first order coordination shell is split into two separate bond distance populations. The chemical composition corresponding to the individual PDFs are presented next to the graphs. For the composition with the lowest B content at the bottom, the solid and dotted vertical lines indicate the maxima, (2.61 and 3.01 Å), of the first and

second bond population, respectively. As observed in Fig. 3.11, both maxima shift continuously to higher distances with increasing B content from bottom to top. Peak positions of the first and second maxima for the highest B content are at 2.63 and 3.05 Å, (respectively), which yields a chemically induced change in relative bond distance of more than 1 %. The error by deconvolution on the measured bond population maxima is below 0.1 % in relative bond distance. By correlation with literature data on the Co-Zr-Ta-B metallic glass system[69], where the bond distance derived from the atomic radii for a Co-Co first order bond length is 2.5 Å and the Zr-Zr first order bond distance is reported to be 3.2 Å, it is inferred that the first bond population (see Fig. 3.11) corresponds to Co-Co first order bonding, whereas the second bond population is dominated by Zr-Zr bonding. As expected, no prior peak around 2 Å is measured[30,73]. Hence, no metal to B and B to B bonds are visible in the measured PDFs. This can be attributed to the larger weighting factor[7,69] of the metals compared to B. Therefore, no direct structural information on the B topology can be obtained experimentally. However, the B content induced changes in metal-to-metal topology are directly accessible by scattering experiments. As previously mentioned, the first order Co-Co and Zr-Zr bond populations shift to higher bond distances as the B content is increased. An increasing bond distance causes bond weakening[88]. Thus, the here reported B-induced structural evolution validates the *ab initio* investigations by Gu *et al.*[67], predicting a metalloid-content-induced metal-to-metal bond weakening.

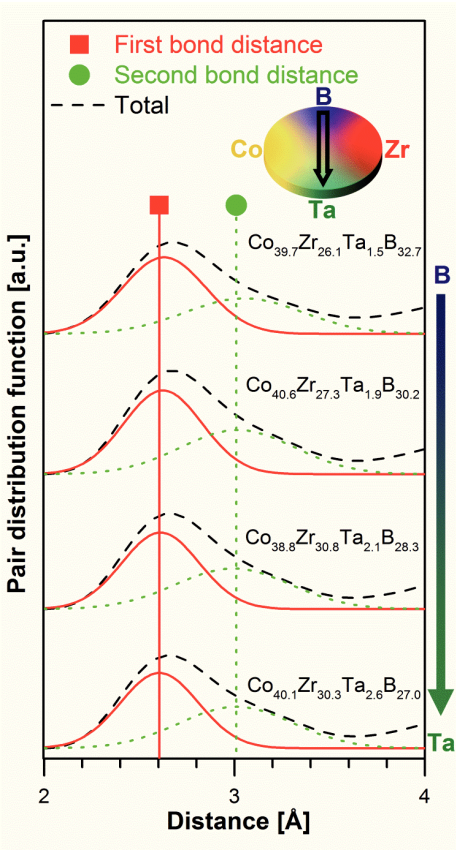

Figure 3.11: Pair distribution functions with increasing B-content from bottom to top obtained by high energy X-ray diffraction are presented in a range between 2 to 4 Å. Next to the total pair distribution functions, the first and second bond population distributions are included, which are obtained by Gaussian peak deconvolution.

The PDFs obtained along the Co-Zr concentration gradient are investigated next to evaluate the metallic content-induced topological evolution. The PDFs with increasing Co content from bottom to top obtained by high energy X-ray diffraction are presented in a range between 1.5 to 10.5 Å in Fig. 3.12. The PDF at the bottom is

obtained for the highest Zr content, whereas the PDF at the top is obtained for the highest Co content.

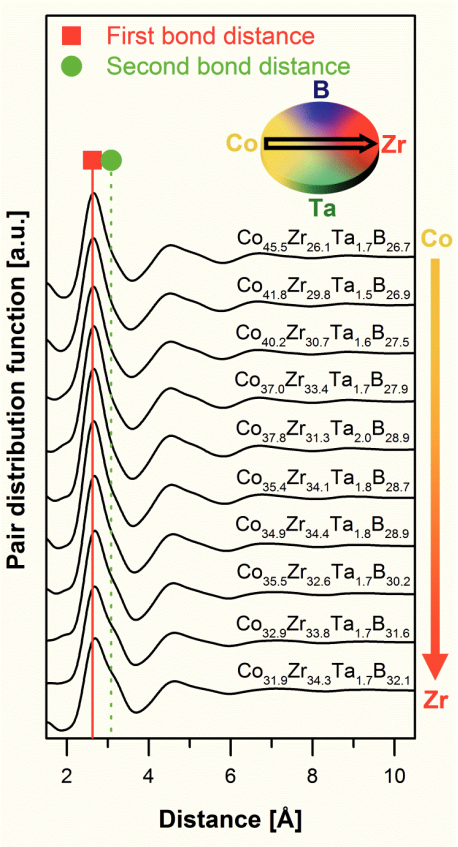

Figure 3.12: The pair distribution functions with increasing Co content from bottom to top obtained by high energy X-ray diffraction are presented in a range from 1.5 to 10.5 Å. The data at the bottom were obtained for the highest Zr content, whereas the data at the top were acquired for the highest Co content. The peak with the maximum amplitude represents the first order coordination shell.

The first peak at around 2.6 Å corresponds to the first order coordination shell, while the second, located between 3.7 and 6.0 Å, corresponds to the second order

coordination shell. It is observed that a shoulder to the right of the first coordination shell peak appears as the Zr content is increased. This shoulder can be attributed to the Zr-Zr dominated bond population, which is consistent with the increase in Zr concentration along the Co-Zr gradient. In addition to the increase in bond population, a shift towards higher bond distances of about 3 % is observed (see Fig. 3.12). Hence, it can be inferred that an increasing Zr content leads to a large population of Zr-Zr bonds. In order to further evaluate the topological splitting of the first coordination shell peak into Co-Co and Zr-Zr bond populations, spatially resolved chemical analysis is performed by APT. In Fig. 3.13 an APT image of the Co-Zr-Ta-B thin film is presented in part a), where the spatially resolved chemical analysis along the cylinder is presented in part b). The APT measurement is conducted along the film growth direction. Iso-surfaces with the concentrations of 50.00 at.% for Co and 28.32 at.% for Zr are displayed in the APT image. It can be observed that nanoscale Co and Zr-rich phases are formed. The maximum compositional difference between these two phases is about 15 at.% for Co (see Fig. 3.13b). Fig. 3.13c indicates that the measured (open circles) and the ideal (lines) distributions do not correspond. The p-value shows the probability of obtaining the observed reduced χ^2 with a confidence level of 99 %. The p-values <0.0001 for all four elements strongly imply the non-randomness of the ion distribution. This separation in Co and Zr rich phases is consistent with the observed separation of the Co-Co and Zr-Zr bond population induced by an increase in Zr content. Hence, the notion regarding the presence of amorphous Co rich and Zr rich phases, which is suggested based on the topology analysis, is also supported by the spatially resolved chemical analysis.

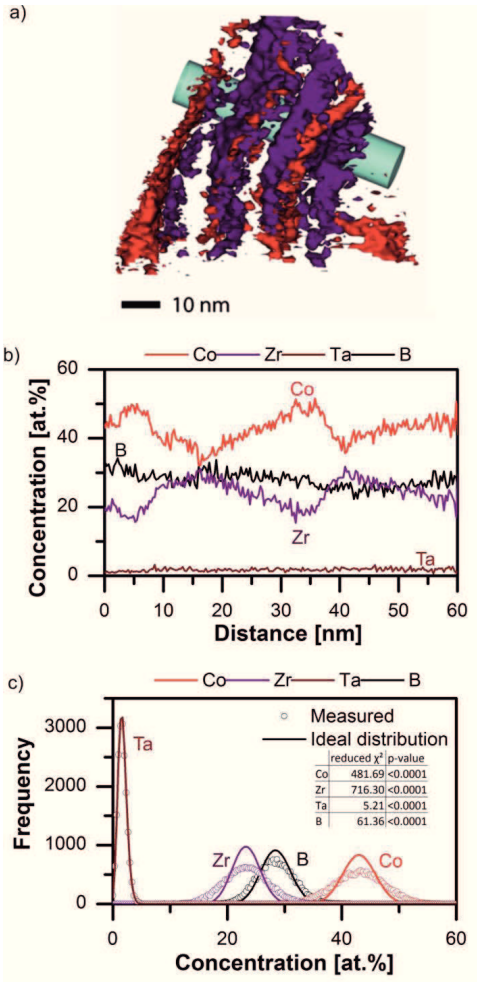

Figure 3.13: a) An atom probe tomography image of the Co-Zr-Ta-B metallic glass is presented including the iso-concentration surfaces of 50.00 at.% for Co and 28.32 at.% for Zr. The APT measurement is conducted along the film growth direction. Along the cylinder (→ direction) the concentration profile for Co, Zr, Ta and B is obtained and provided in b). c) A frequency distribution function for the data obtained in a) is presented. The inset table shows the deviation between the ideal (lines) and the measured (open circles) distribution, such that the p-values indicate a non-random chemical distribution[89].

In contrast to the micrometer sized phase separation observed in bulk metallic glasses[90,91], the composition modulation observed here exhibits a periodicity of 20-30 nm perpendicular to the film growth direction. The chemical distribution observed suggests that the high quenching rates[92] present in physical vapour deposition retard diffusion and consequently impede the evolution of long range order, as well as composition modulations, on length scales larger than the a few nm[90,91]. Nevertheless, the presence of chemical modulation on the nm scale may be explained by limited surface diffusion, (on the nm scale), enabled by the interaction of the energetic sputtered flux with the growing film surface[93]. Therefore, it is inferred that the combination of high quenching rates and limited ad-atom mobility enables the evolution of composition modulations on the nm length scale. To evaluate the chemistry – topology – stiffness relationship, the chemically induced topology changes will next be correlated to the reduced Young's moduli obtained by nanoindentation.

Chemistry – topology – stiffness relationship

For the evaluation of the chemistry – topology – stiffness relationship the topological and reduced Young's moduli are depicted along the Co-Zr and B-Ta concentration gradients in Fig. 3.14. In the centre of Fig. 3.14, the position of the first and second maxima of the metal- to-metal bond distance population is presented to the left and to the right, respectively. The distance of the first bond population maxima ranges from 2.61 to 2.63 Å. The distance of the second bond population maxima ranges from 2.99 to 3.08 Å, which is a variation of 3 % in relative bond distance. For the second bond population maxima, the error by deconvolution is below 1 %.

At the bottom of Fig. 3.14 the reduced Young's modulus and the schematic deposition setup are depicted to the left and right, respectively. The reduced Young's

modulus varies between 183 to 203 GPa. Applying a Poisson's ratio[30] of 0.28 to the reduced Young's moduli obtained by nanoindentation, Young's moduli in the range of 201 to 227 GPa are obtained, which is smaller compared to 268 GPa reported for the Co-Fe-Ta-B system[5]. Due to the smooth surface of the metallic glass thin film, the standard deviations of the stiffness measurements are between 3 and 6 GPa for each set of the 24 indentation measurements per composition. Thus, the observed increase in stiffness is statistically significant. The same conclusion can be drawn from Fig. 3.15 where the reduced Young's modulus measured along the B-Ta concentration gradient is presented as a function of B content including the error bars for the individual sets of stiffness measurements.

It is observed from the reduced Young's modulus data in Fig. 3.14 that the stiffness increases almost continuously along both, the Ta to B and the Co to Zr concentration gradients. Along these concentration gradients the bond distances of Co-Co and Zr-Zr increase. Hence, the shortest Co-Co and Zr-Zr bond distances correspond to regions with the lowest Young's modulus, which is contradictory to the notion that shorter bond distances or in other words denser metal-to-metal packing causes an increase in bond stiffness[88]. For metallic glasses not containing metalloids it has been reported that denser packing leads to an increase in stiffness[94]. However, for the here studied metal – metalloid Co-Zr-Ta-B metallic glass thin film the metalloid concentration dominates stiffness. This observation is in agreement to the observations made by Wang *et al.*[48] and Hostert *et al.*[30], who propose strong, hybridised metal-B bonds to cause high stiffness of Co-based metallic glasses. It is reasonable to assume that with an increasing B content from 26.7 to 32.7 at.% the fraction of hybridised metal-to-metalloid bonds increases, which is in line with the here measured stiffness data.

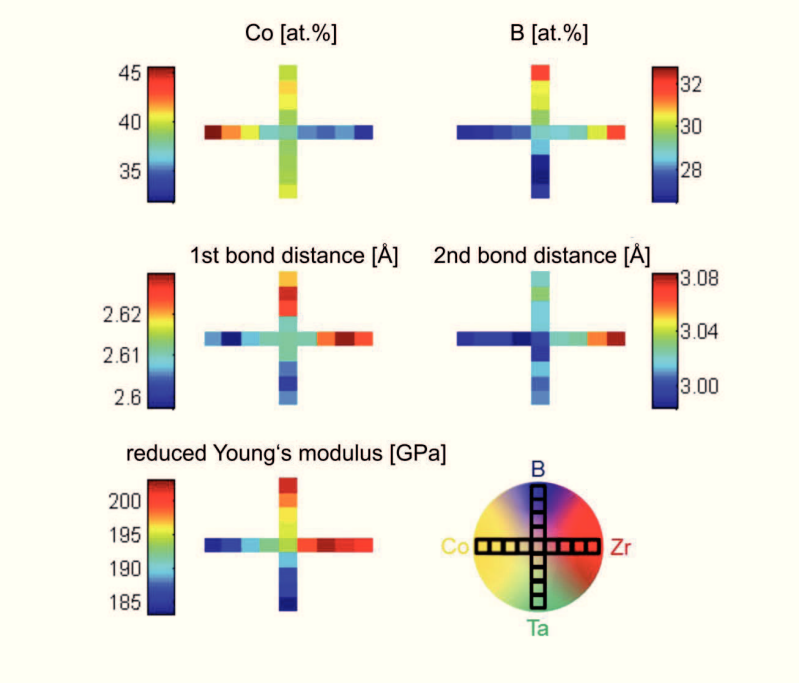

Figure 3.14: The compositional, structural and stiffness measurements along the concentration gradients are depicted. At the top, the Co and B compositions are presented. In the center, maxima of the first and second metal-to-metal bond distance populations are given to the left and to the right, respectively. At the bottom, the reduced Young's modulus and the corresponding deposition schematic deposition is depicted to the left and right, respectively.

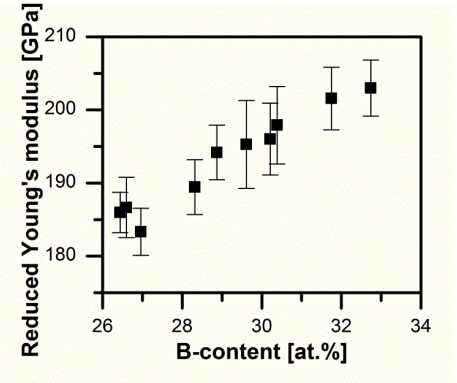

Figure 3.15: The reduced Young's modulus is presented as a function of B-content. It is observed that with increasing B-content the reduced Young's modulus increases.

3.4 Damage-tolerant glasses

Demetriou *et al.* reported a damage-tolerant metallic glass that combines strength and toughness beyond the benchmark ranges established by any known material[2]; however, its underlying physical and chemical mechanisms are not understood on the atomic scale. Current alloy design guidelines for metallic glasses are based on the notion of a clear and universal relationship between Poisson's ratio and fracture energy to define the brittle-ductile transition[3,4].

To identify the chemical origin for the toughness of metallic glasses, the design proposal of Lewandowski *et al.*[3] and Greaves *et al.*[4] is critically appraised using a correlative *ab initio* molecular dynamics and *in situ* micro mechanical testing approach while also considering the literature data[4-6]. Here, metallic glass thin films are synthesised by physical vapour deposition[73], exhibiting a Poisson's ratio range from 0.29 to 0.37.

Park *et al.*[95] showed that chemical inhomogeneity may cause embrittlement of metallic glasses and alter their mechanical response. Hence, the chemical homogeneity of all thin film metallic glasses presented in Fig. 3.17 are investigated by atom probe tomography. Fig. 3.16 shows as an example the tomography and frequency distribution analysis[9] of $Pd_{57.0}Al_{23.9}Cu_{11.4}Y_{7.7}$ glass[96]. It is evident that all alloying constituents are randomly distributed, and hence no strain localization is expected. The ideal chemical homogeneity may be due to the large quenching rates typical of physical vapour-deposited thin film metallic glasses[92].

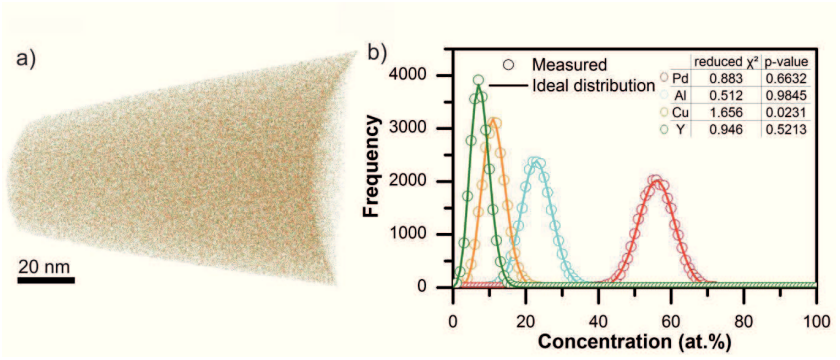

Figure 3.16: Preventing chemical-inhomogeneity-induced local catastrophic shear banding is essential for high damage tolerance. a) The spatially resolved chemical analysis by atom probe tomography reveals a homogeneous chemical distribution throughout the specimen. As an example, the results for the $Pd_{57.0}Al_{23.9}Cu_{11.4}Y_{7.7}$ glass are shown. The other glasses, which are not presented here, exhibit a homogeneous chemical distribution as well. b) The ideal chemical distributions for the present concentration are displayed as lines; the measurement, which is in very good agreement with the ideal distribution, is represented by the open symbols. The inset table shows the deviation between the ideal and measured distribution; the p-value indicates its randomness[89].

The mechanical behaviours of the thin film metallic glasses are examined by micro-fracture experiments[12,13], as presented in Fig. 3.17. The load-displacement curves for two representative examples of marginally damage-tolerant $Cu_{67.8}Zr_{32.2}$ and highly damage-tolerant $Pd_{57.0}Al_{23.9}Cu_{11.4}Y_{7.7}$ glass, both exhibiting the same Poisson ratio, are depicted in Fig. 3.17d in blue and red, respectively. The marginally damage-tolerant glass shows pure elastic deformation before abrupt, catastrophic fracture at a peak load from which the fracture toughness (2.7 $MPam^{1/2}$) and fracture energy (0.06 kJ/m^2) were determined using linear elastic fracture mechanics[16].

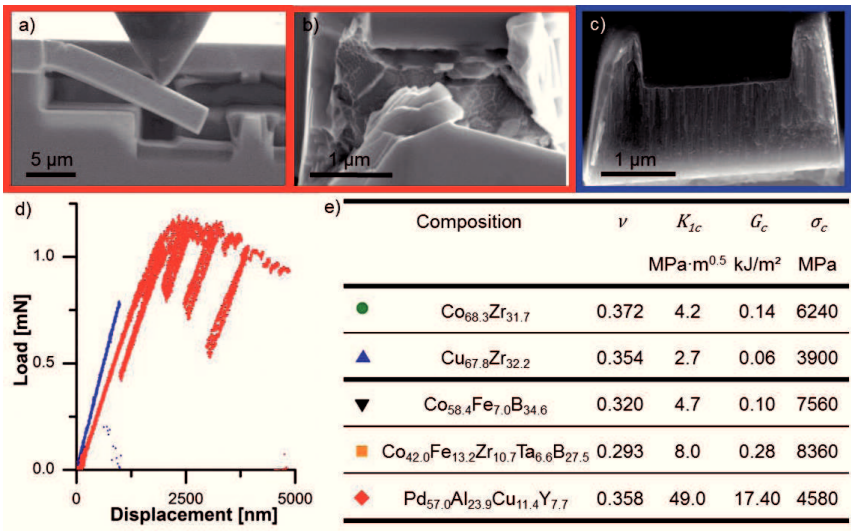

e)

Composition	ν	K_{1c}	G_c	σ_c
		MPa·m$^{0.5}$	kJ/m²	MPa
$Co_{68.3}Zr_{31.7}$	0.372	4.2	0.14	6240
$Cu_{67.8}Zr_{32.2}$	0.354	2.7	0.06	3900
$Co_{58.4}Fe_{7.0}B_{34.6}$	0.320	4.7	0.10	7560
$Co_{42.0}Fe_{13.2}Zr_{10.7}Ta_{6.6}B_{27.5}$	0.293	8.0	0.28	8360
$Pd_{57.0}Al_{23.9}Cu_{11.4}Y_{7.7}$	0.358	49.0	17.40	4580

Figure 3.17: *In situ* micro-cantilever deflection experiments. The fracture strength and toughness of the metallic glass thin films are measured by employing both un-notched and pre-notched specimens. a) Representative scanning electron image of an *in situ* micro-cantilever deflection experiment performed on a $Pd_{57.0}Al_{23.9}Cu_{11.4}Y_{7.7}$ glass. b) and c) show high magnification images of the crack trajectory and fracture surface of the tough $Pd_{57.0}Al_{23.9}Cu_{11.4}Y_{7.7}$ and the brittle $Cu_{67.8}Zr_{32.2}$ metallic glass, respectively. d) Load-displacement graphs for the brittle $Cu_{67.8}Zr_{32.2}$ in blue and the tough $Pd_{57.0}Al_{23.9}Cu_{11.4}Y_{7.7}$ in red. The dissipated energy before fracture (area under the curve) for the highly damage tolerant $Pd_{57.0}Al_{23.9}Cu_{11.4}Y_{7.7}$ glass is much higher compared to the brittle $Cu_{67.8}Zr_{32.2}$ glass. e) Summary of the *ab initio* calculated Poisson's ratio (ν), and the measured quantities fracture toughness (K_{1c}), fracture energy (G_c) and fracture strength (σ_c) of the glasses studied within this work.

In contrast, the more damage-tolerant $Pd_{57.0}Al_{23.9}Cu_{11.4}Y_{7.7}$ glass exhibits extensive plastic deformation in the form of shear bands leading to significant energy dissipation before fracture[1]. Therefore, elasto-plastic fracture mechanics via J-integral analysis[12] were applied to quantify the damage tolerance. The determined fracture toughness (49 $MPam^{1/2}$) and fracture energy (17.4 kJ/m^2) significantly exceed the values of the brittle $Cu_{67.8}Zr_{32.2}$ glass. A snapshot from the *in situ* scanning electron microscopy bending experiment of the $Pd_{57.0}Al_{23.9}Cu_{11.4}Y_{7.7}$ thin film metallic glass is provided in Fig. 3.17a. The fracture surfaces of the two glasses are shown in Fig. 3.17b-c and conform to the known topographies of ductile (large dimples) and brittle (fine features) metallic glass, respectively. The outstanding damage tolerance of the glasses investigated here compared to other material classes[12,14,15] is evident in Fig. 3.17e and 3.18. The fracture energy is depicted as a function of the calculated Poisson's ratio for the five thin film metallic glasses studied here and the 29 other glasses from the literature[2,4,5,16-22]. The oxide glasses[2,19] with a Poisson's ratio of 0.266 and lower exhibit low toughness with a fracture energy below 0.01 kJ/m^2. The Fe-based metallic glasses display a systematic change in Poisson's ratio from 0.314 to 0.330, which is chemically induced[97]. The last three thin film metallic glasses in Fig. 3.17e are consistent with the present alloying guidelines[3,4], whereas the first two thin film metallic glasses in Fig. 3.17e exhibit Poisson's ratios of 0.354 to 0.372 and brittle behaviour. These Poisson's ratios are much higher compared to the proposed sharp brittle-to-tough transition range[3] of 0.31–0.32. The three order of magnitude difference in fracture energy between the tough $Pd_{57.0}Al_{23.9}Cu_{11.4}Y_{7.7}$ and the brittle $Cu_{67.8}Zr_{32.2}$ metallic glasses with identical Poisson's ratios is in conflict with the proposed universal relationship between Poisson's ratio and fracture energy[3,4].

Furthermore, it can be seen in Fig. 3.18b that the Zr-based metallic glasses exhibit two separate distributions of toughness dependence within the same range of Poisson's ratio[98,99]. The Zr-based metallic glasses without Ni (☆)[99] exhibit toughness values exceeding 140 kJ/m^2, whereas the Zr-based metallic glasses containing Ni (◌)[98,99] possess toughness values ranging from 0.06 to 39 kJ/m^2. In addition, there are literature reports on Pd-based metallic glasses that exhibit a brittle-to-tough evolution within a narrow Poisson's ratio range[6] of 0.39–0.41. Hence, it is evident from here presented and literature data that the Poisson's ratio range of 0.31 to 0.32 does not accurately gauge the brittle-to-ductile transition.

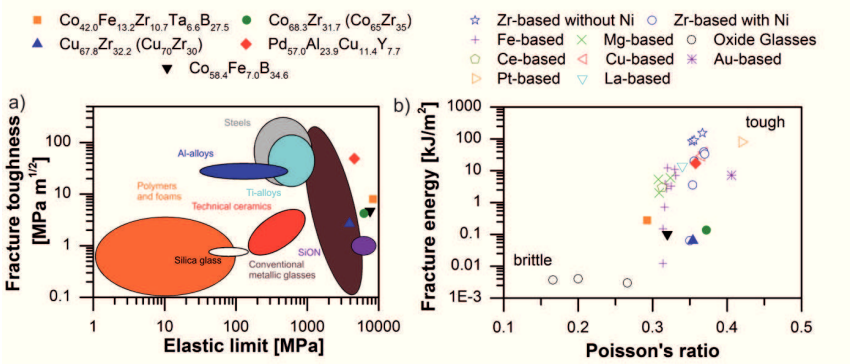

Figure 3.18: Experimental validation reveals extraordinary damage tolerance for the metallic glasses studied in this work. a) The fracture strength of the glasses studied in this work is close to the ideal strength of the material. The $Pd_{57.0}Al_{23.9}Cu_{11.4}Y_{7.7}$ thin film metallic glass is identified to exhibit high damage tolerance. b) Poisson's ratio cannot gauge the chemical origin of the rapid evolution from brittle to tough behaviour. Literature data for the Mg-based, Ce-based and La-based[16,17], Fe-based[97], oxide glasses[2,19], Zr-based[98,99], Cu-based[20,21], Pt-based[100] and Au-based[101] glasses are presented.

To investigate the chemical origin for the observed evolution from brittle to ductile behaviour, electronic density-of-state analysis is used to probe the bonding states of all five glass compositions in detail. The results of two glass compositions that have identical Poisson's ratios but exhibit the largest difference in fracture energies: the tough $Pd_{57.0}Al_{23.9}Cu_{11.4}Y_{7.7}$ and the brittle $Cu_{67.8}Zr_{32.2}$ are presented in Fig. 3.19. Comparing the partial density of states for Cu and Zr to the total density of states (Fig. 3.19a), it can be observed that there is a strong hybridisation in the deep core states at approximately –4 eV. A completely different bonding behaviour can be observed for the $Pd_{57.0}Al_{23.9}Cu_{11.4}Y_{7.7}$ glass depicted in Fig. 3.19c. With Pd and Al as the two main constituents of this glass populating different energy levels, the overall degree of hybridisation is low. Thus it is proposed that solids with a small contribution of hybridised bonds to the overall bond character and therefore less directional bonding and less topological connectivity resist a volume change in favour of a shape change by shear. Hence, it can be inferred that with Pd and Al populating different energy levels, the species are more likely to accommodate shear and facilitate the generation of shear transformation zones[58]. This notion is consistent with the fracture surface analysis and fracture toughness data presented here. The outcome of the electronic structure comparison is that hybridisation is the predictor for high damage tolerance in glasses. Additionally, to evaluate the change of bonding nature upon deformation, the density of states is studied in a sheared state. For the $Cu_{67.8}Zr_{32.2}$ glass exposed to 5 % shear, the centre of mass for the total density of states shifts by only 0.05 eV compared to the unstrained glass. On the other hand, the total density of states in the $Pd_{57.0}Al_{23.9}Cu_{11.4}Y_{7.7}$ glass exposed to 5 % shear shifts by 0.3 eV towards the Fermi level. Hence, the glass becomes softer upon shearing, which explains the onset of plasticity and the high toughness observed. Based on correlative theoretical and experimental data, it is evident that the fraction of bonds

stemming from deep core, hybridised states compared to the overall bonding can serve as a measure for damage tolerance, reflecting the electronic nature of the mechanisms involved. A low fraction of hybridised states yields easy shear relaxation, thus promoting the formation of shear transformation zones, which initiates plastic deformation and bond switching. This notion is supported not only by here presented data but also by published literature on the electronic structure of Zr-Ni-Al metallic glasses[99], in which directional covalent bonding between Ni and Al is identified to induce a decrease in toughness (Fig. 3.18b). In contrast to the notion of a sharp transition from brittle to ductile behaviour within a Poisson's ratio range from 0.31 to 0.32[3], a design principle for damage-tolerant glasses that rests firmly on an in-depth understanding of the electronic structure is provided. The fraction of bonds stemming from deep core, hybridised states compared to the overall bonding is identified as the chemical origin for the outstanding damage-tolerance of $Pd_{57.0}Al_{23.9}Cu_{11.4}Y_{7.7}$ with a strength exceeding 4 GPa and fracture toughness of 49 $MPam^{1/2}$, which is one order of magnitude larger than that of ultrahigh-strength glasses[5].

Whereas Poisson's ratio alone is not a sufficient criterion to determine the brittle-ductile transition of glasses, it constitutes a valuable alloying guideline and is hence an important first-order material design criterion. By unravelling the chemical origin of the transition from brittle to tough behaviour at the electronic structure level, this work enables knowledge-based design of novel damage-tolerant metallic glasses using computer-assisted simulation predictions while explaining previous reports of deviation from expected behaviour.

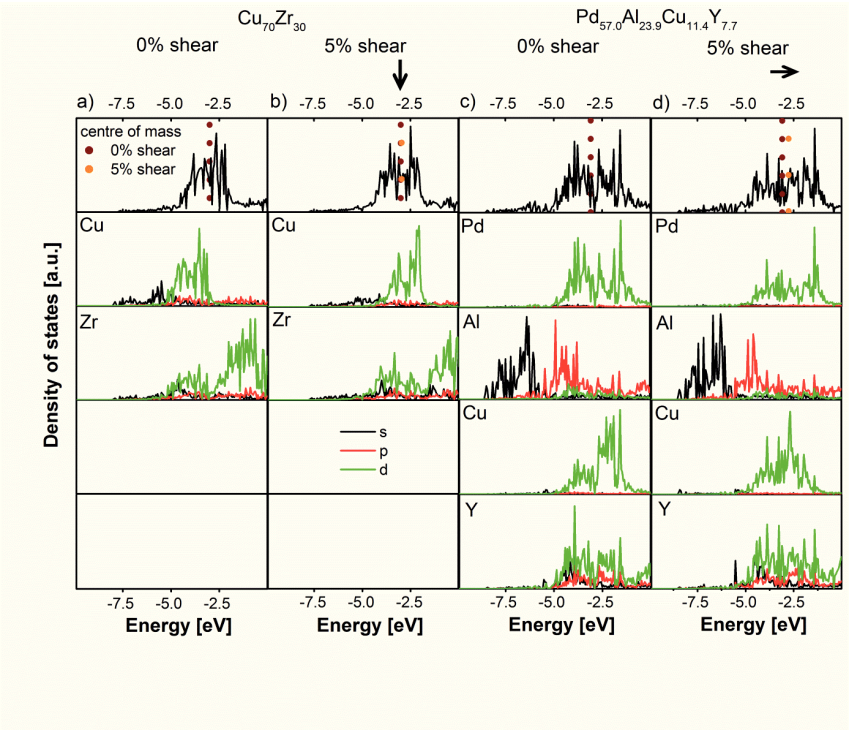

Figure 3.19: Fraction of bonds stemming from deep core, hybridised states compared to the overall bonding defines damage tolerance in glasses. The s, p and d orbitals are presented in black, red and green, respectively. The Fermi level for each glass is set to zero. The energy levels down to –10 eV are presented. The arrows indicate the shift of the centre of mass for the total density of states.

4 Conclusions

In situ high-temperature X-ray diffraction experiments using high-energy photons and *ab initio* molecular dynamics simulations are performed to probe the temperature induced changes in topological short-range order in magnetron sputtered $Co_{67}B_{33}$ metallic glass thin films. Good agreement between the experimentally obtained PDFs and the PDFs obtained by *ab initio* MD simulation is observed. The loss in coherence between the first and second Co-B coordination shell together with the evolution of the B-B coordination is inferred based on the observed temperature induced decrease in population of rigid second order B-Co-B building blocks. This interpretation is also consistent with the thermally induced decrease in population of densely packed Frank-Kasper like polyhedra, which was obtained by Voronoi tesselation. The here reported temperature induced changes in topological and chemical order cause an increase in the population of ready to flow regions inferring a transition from a localized shear band dominated deformation mode to a homogeneous deformation mode, which may explain the extensive temperature dependence of the elastic limit reported previously. The here reported temperature induced changes in topological and chemical order may be exploited in future materials design efforts to enhance ductility of these very stiff solids stabilizing ready to flow regions at lower temperature by alloying.

After evaluating the temperature induced brittle to ductile transition, the influence of chemical composition on the stiffness and plasticity of Co-Fe-Ta-B metallic glasses by means of *ab initio* molecular dynamic simulations is systematically studied. The $Co_{43.5}Ta_{6.1}B_{50.4}$ composition studied within this work yields the highest stiffness ever reported for a metallic glass. The calculated Young's modulus of 295 GPa is 8 % higher compared to $Co_{43}Fe_{20}Ta_{5.5}B_{31.5}$ metallic glass[30]. The analysis of the total and partial density of states is indicating strong metal to B hybridisation in the region of

-2.5 to -5 eV and -10 eV. Hence strong covalent metal to B bonding is suggested to be the cause for the very high stiffness observed.

It has been reported by Lewandowski *et al.*[3] that the Poisson's ratio of 0.31 to 0.32 marks the transition from brittle to plastic behaviour for metallic glasses. Through employing three different computational strategies, it is determined that by additions of Y, Zr, Nb, Mo, Hf, W, C, N and O the Poisson's ratio can be varied from 0.293 to 0.342. The observed evolution in Poisson's ratio can be attributed to a transition from predominately covalent to predominately metallic bond character, whereas the latter infers a higher tendency towards plastic deformation. Alloying with Zr facilitates similar properties as the $Co_{43}Fe_{20}Ta_{5.5}B_{31.5}$ system, which is an overall brittle behaviour and a large Young's modulus. On the other hand, alloying with N, O, Nb, W and Mo leads to Poisson's ratios above the critical threshold, implying homogeneous deformation, which yields in plastic behaviour. From the analysis of the partial and total density of states for the $Co_{43.5}Fe_{20}Ta_{6.1}B_{15.8}O_{14.8}$ system, a metallically dominated bonding character is predicted, which is consistent with the high Poisson's ratio of 0.340. Thus, it is perceived that the interplay between chemistry and topology affects the mechanical properties of metallic glasses.

To effectively investigate these chemically induced topology changes of thin film metallic glasses, a novel method was introduced to study the chemistry - topology - stiffness relationship of combinatorial thin film metallic glasses. The thin films are deposited on a radiation damage tolerant polyimide foil to enable high energy X-ray diffraction in transmission mode. EDX and APT were used to characterize chemical information along the concentration gradient, while the elastic properties were measured by nanoindentation. A separation into amorphous nanoscale Co and Zr-rich phases is observed by both high energy X-ray diffraction and spatially resolved APT. It is proposed that the formation of composition modulations on the nm scale is

due to the combination of ad-atom mobility, (limited to the nm length scale), and the high quenching rates associated with vapour phase condensation during magnetron sputtering. Furthermore, through the correlative composition and stiffness analysis it is observed that the Co-Zr-Ta-B glass exhibits an increase in stiffness by 10 %, which is induced by an increase in B content from 26.7-32.7 at.%. From the topology analysis along the same chemical gradient, it is understood that as the B content increases, the Co-Co and Zr-Zr first order bond distances increase by 1 %, which implies weakening of bonds. This observation is consistent with *ab initio* studies[67] which predict a metalloid-concentration-induced metal bond weakening. Based on the correlative topology and stiffness analysis along the concentration gradients of a metallic glass thin film, it can be concluded that the B-content-induced increase in hybridisation dominates the corresponding weakening of metallic bonds. So far it can be concluded that hybridisation strongly affects the mechanical properties of Co-based metallic glasses. To evaluate the relevance of hybridisation for metallic glasses in general, alloying guidelines[3,4], delineating a universal relationship between Poisson's ratio and fracture energy are critically appraised by a correlative *ab initio* molecular dynamics and *in situ* micro mechanical approach. The investigated $Co_{42.0}Fe_{13.2}Zr_{10.7}Ta_{6.6}B_{27.5}$, $Co_{58.4}Fe_{7.0}B_{34.6}$, $Co_{68.3}Zr_{31.7}$, $Cu_{67.8}Zr_{32.2}$ and $Pd_{57.0}Al_{23.9}Cu_{11.4}Y_{7.7}$ metallic glass thin films exhibit a Poisson's ratio range from 0.29 to 0.37. It is observed that the $Pd_{57.0}Al_{23.9}Cu_{11.4}Y_{7.7}$ and the $Cu_{67.8}Zr_{32.2}$ metallic glass thin film with Poisson's ratios of 0.358 and 0.354, respectively, show three orders of magnitude difference in fracture energy. Furthermore, there are reports on Pd-based metallic glasses[6], which exhibit a brittle-tough transition in a Poisson's ratio range of 0.39-0.41. Hence, it is evident from our data and literature data that the Poisson's ratio range of 0.31 to 0.32 does not accurately gauge the brittle-to-ductile transition. Density of states analysis reveal that the brittle $Cu_{67.8}Zr_{32.2}$ metallic glass exhibits

deep core hybridisation at approximately -4 eV, whereas the Pd and Al as the two main constituents of the $Pd_{57.0}Al_{23.9}Cu_{11.4}Y_{7.7}$ glass populate different energy levels. Hence, it is proposed that an overall lower fraction of bonds stemming from deep core, hybridised states induces less directional bonding and hence, less topological connectivity, which facilitates the generation of shear transformation zones and tough behaviour. Hence, contrary to current alloying guidelines, damage tolerance is defined by the overall fraction of bonds stemming from deep core, hybridised states.

5 Future work

Even though, as reported in literature[8] Co-based metallic glasses exhibit extraordinary magnetic properties, this work focuses on the outstanding mechanical properties of metallic glasses. However, as reported here, the topology and electronic structure is strongly determined by chemical composition. Especially, an increase in B content induces severe changes in bond character. It is proposed that through correlative *ab initio* molecular dynamics simulations and superconducting quantum interference device measurements the B induced evolution of magnetisation can be investigated in order to obtain a better understanding of the topology, electronic structure and magnetic property relationship of these fascinating materials.

Additionally the conclusion that a small contribution of hybridised bonds to the overall bond character is essential for damage tolerant glasses raises the question, if this notion is also generally relevant for oxide glasses. It is proposed to systematically explore the influence of oxygen content of inorganic oxide glasses on the electronic structure-topology-mechanical properties relationship by a combination of thin film synthesis, molecular dynamics simulations, high energy XRD and micro mechanical testing.

To further enhance the damage tolerance of metallic glasses, the key element is to control shear band nucleation and propagation, as they govern plastic deformation in glasses. Here two scientific strategies are proposed for the design of novel damage-tolerant glasses. The first scientific strategy focuses on further developing and validating the design strategy proposed within this thesis. It has been shown that the fraction of bonds stemming from deep core, hybridised states compared to the overall bonding defines damage-tolerance in glasses. Furthermore, it has been observed that the degree of hybridisation is chemically induced. Hence, it is proposed that

through alloying, the contribution of hybridised bonds to the overall bond character can be reduced, which therefore causes less directional bonding and less topological connectivity. As a starting point the already outstanding damage-tolerant $Pd_{57.0}Al_{23.9}Cu_{11.4}Y_{7.7}$ metallic glass can be chosen. It is proposed that through the substitution of the hybridising Cu and Y with more noble elements e.g. Pt, Au or Ir the topological connectivity can be reduced. Thus, by adjusting the chemistry, easy shear band formation can be promoted, which is expected to enhance damage-tolerance.

The second scientific strategy proposed focuses on controlling both the shear band nucleation and propagation by designing metallic glasses, which are geometrically constrained on the nm scale. It has been shown by Pan *et al.*[102] that the ductility of metallic glasses is correlated to the volume of active shear transformation zones, which exhibit volumes below 10 nm^3. Futhermore, is has been reported that the tendency towards shear band formation is not only chemistry but also sample size dependent[58,103]. Hence, for small sample sizes the shear band generation becomes deformation rate limiting and the strength of a metallic glass can be increased by decreasing the sample size towards the nanometer scale[58]. Here it is proposed that by designing nanolaminated metallic glasses with a layer thickness below the size of shear transformation zones, shear band nucleation can be surpressed, which infers an increase in elastic limit. On the other hand, it is proposed here that nanolaminated metallic glasses with domain sizes slightly large than shear transformation zones (e.g. a few thenth of nm) shear band propagation can be guided along these domains, by which the coalescence of shear bands can be surpressed inducing an increase in plasticity. It is suggested to systematically explore the influence of domain size on shear-band nucleation and propagation using layer thickness graded nanolaminates, synthesised by combinatorial physical vapour deposition (Fig. 5.1).

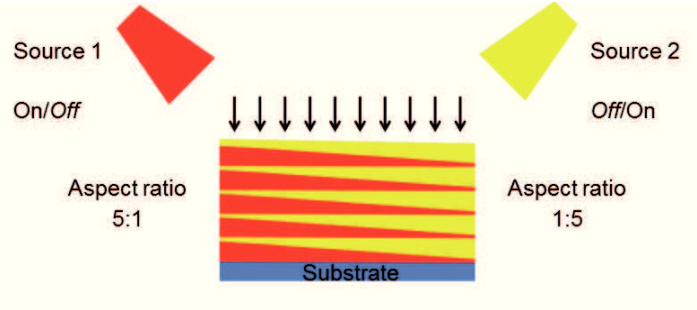

Figure 5.1: Schematic of combinatorical thickness graded nanolaminate with varying layer aspect ratio from left to right. The variation in aspect ratio is achieved by combinatorial deposition at an angle of 45° normal to the substrate. Along this aspect ratio gradient the mechanical properties can be investigated by e.g. nanoindentation, which is indicated by the arrow pattern.

Through deposition from individual sources at an angle of 45° normal to the substrate, layer thickness graded nanolaminates can be designed. Hence, the geometrical constrain, imposed by the second phase of the nanolaminate can systematically vary across the sample. Through micro mechanical experiments e.g. pillar compression tests or nanoindentation the mechanical properties of these thin films can be investigated along the thickness gradient, where the aspect ratio is systematically varied. This systematic approach, enabled by combinatorial thin film synthesis, is proposed to be most efficient for understanding and crontrolling the geometrical constraint induced shear band nucleation and propagation. A schematic drawing of the ultra-high vaccum system currently being designed and built at Materials Chemistry, RWTH Aachen is depicted in Fig. 5.2. The system consits of a load lock system and a main synthesis chamber equipped with a substrate holder (blue), three magnetron sources (red) and the associated fast acting shutters (yellow), which enable the synthesis of thickness graded nanolaminates.

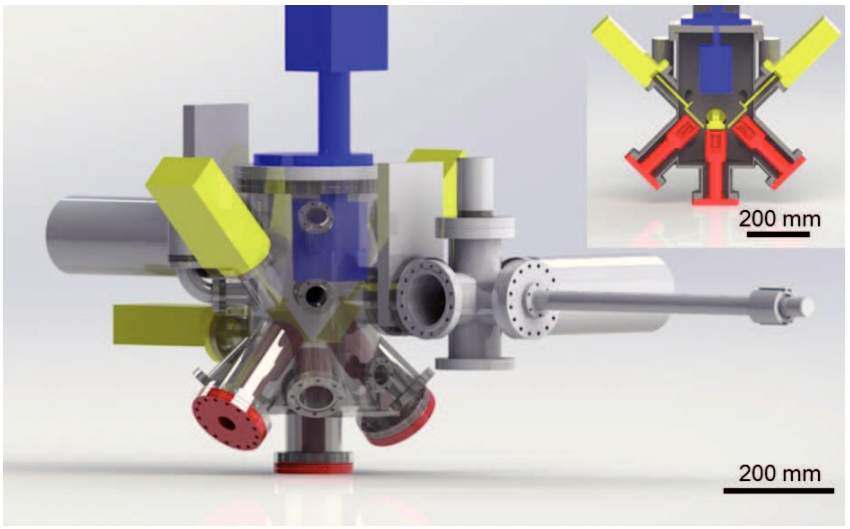

Figure 5.2: Schematic drawing of the ultra-high vacuum chamber currently being designed and built at Materials Chemistry, RWTH Aachen. The individual sputter sources, substrate holder and fast target shutters are depicted in red, blue and yellow, respectively. The inset at the top right shows the magnetron and shutter arrangement as a cross sectional view of the main chamber body.

6 References

[1] Schuh, C.A., Hufnagel, T.C., & Ramamurty, U., Mechanical behavior of amorphous alloys. *Acta Mater.* 55, 4067-4109 (2007).

[2] Demetriou, M.D., Launey, M.E., Garrett, G., Schramm, J.P., Hofmann, D.C., Johnson, W.L., & Ritchie, R.O., A damage-tolerant glass. *Nature Mater.* 10, 123-128 (2011).

[3] Lewandowski, J.J., Wang, W.H., & Greer, A.L., Intrinsic plasticity of brittleness of metallic glasses. *Philos. Mag. Lett.* 85, 77-87 (2005).

[4] Greaves, G.N., Greer, A.L., Lakes, R.S., & Rouxel, T., Poisson's ratio and modern materials. *Nature Mater.* 10, 827-837 (2011).

[5] Inoue, A., Shen, B.L., Koshiba, H., Kato, H., & Yavari, A.R., Ultra-high stength above 5000 MPa and soft magnetic properties of Co-Fe-Ta-B bulk glassy alloys. *Acta Mater.* 52 (52), 1631-1637 (2004).

[6] Kumar, G., Prades-Rodel, S., Blatter, A., & Schroers, J., Unusual brittle behavior of Pd-based bulk metallic glass. *Scripta Mater.* 65, 585-587 (2011).

[7] Kaban, I., Jovari, P., Stoica, M., Eckert, J., Hoyer, W., & Beuneu, B., Topological and chemical ordering in $Co_{43}Fe_{20}Ta_{5.5}B_{31.5}$ metallic glass. *Phys. Rev. B* 79, 212201 (2009).

[8] Inoue, A., Shen, B., & Takeuchi, A., Developments and Applications of Bulk Glassy Alloys in Late Transition Metal Base System. *Matr. Trans.* 47, 1275-1285 (2006).

[9] Inoue, A., Stabalization of metallic supercooled liquid and bulk amorphous alloys. *Acta Mater.* 48, 279-306 (2000).

[10] Ishida, M., H.Takeda, Watanabe, D., Amiya, K., N.Nishiyama, Kita, K., Saotome, Y., & Inoue, A., Fillability and Imprintability of High-strength Ni-based Bulkd Metallic Glass Prepared by the Precision Die-casting Technique. *Matr. Trans.* 45, 1239-1244 (2004).

[11] Hata, S., Kato, T., Fukushige, T., & Shimokohbe, A., Integrated conical spring linear actuator. *Microelectron. Eng.* 67-68, 574-581 (2003).

[12] Ashby, M.F. & Greer, A.L., Metallic glasses as structural materials. *Scripta Mater.* 54, 321-326 (2006).

[13] Wu, F.F., Zheng, W., Deng, J.W., Qu, D.D., & Shen, J., Super-high compressive plastic deformation behaviors of Zr-based metallic glass at room temperature. *Mater. Sci. Eng., A* 541, 199-203 (2012).

[14] Ashby, M.F. ed., Materials Selection in Mechanical Design, Third edition ed. (Elsevier Butterworth-Heinemann, Linacre House, Jordan Hill, Oxford, 2005).

[15] Dahl, W. & Anton, W. eds., Werkstoffkunde Eisen und Stahl. (Verlag Stahleisen mbH, Düsseldorf, 1983).

[16] Matoy, K., Schönherr, H., Detzel, T., Scöberl, T., Pippan, R., Motz, C., & Dehm, G., A comparative micro-cantilever study of the mechanical behavior of silicon based passivation films. *Thin Solid Films* 518, 247-256 (2009).

[17] Kramme, R. ed., Medizintechnik Verfahren – Systeme – Informationsverarbeitung. (Springer Medizin Verlag, Heidelberg, 2007).

[18] Inoue, A., Shen, B., & Takeuchi, A., Fabrication, properties and applications of bulk glassy alloys in late transition metal-based systems. *Mater. Sci. Eng., A* 441, 18-25 (2006).

[19] Rouxel, T., Elastic Properties and Short-to Medium-Range Order in Glasses. *Journal of the American Ceramic Society* 90 (10), 3019-3039 (2007).

[20] Pugh, S.F., Relations between the Elastic Moduli and the Plastic Properties of Polycrystalline Pure Metals. *Philos. Mag.* 45, 823-843 (1954).

[21] Argon, A.S., Plastic deformation in metallic glasses. *Acta Matall.* 27 (1), 47-58 (1979).

[22] Sholl, D.S. & Steckel, J.A. eds., Density functional theory. (John Wiley & Sons, Hoboken, New Jersey, 2009).

[23] Hohenberg, P. & Kohn, W., Inhomogeneous Electron Gas. *Phys. Rev.* 136, 864-871 (1964).

[24] Perdew, J.P., in *Electronic structure of solids '91*, edited by Paul Ziesche & H. Eschrig (Akademie Verlag, Berlin, 1991), pp. 11.

[25] Monkhorst, H.J. & Pack, J.D., SPECIAL POINTS FOR BRILLOUIN-ZONE INTEGRATIONS. *Phys. Rev. B* 13 (12), 5188-5192 (1976).

[26] Ozaki, T. & Kino, H., Efficient projector expansion for the ab initio LCAO method. *Phys. Rev. B* 72, 045121 (2005).

[27] Kresse, G. & Fürthmüller, J., Efficient iterative schemes for *ab initio* total-energy calculations using a plane-wave basis set. *Phys. Rev. B* 54, 11169 (1996).

[28] Sholl, D.S., *Density functional theory: a practical introduction*. (John Wiley & Sons, Inc., 2009).

[29] Ozaki, T., Variationally optimized atomic orbitals for large-scale electronic structures. *Phys. Rev. B* 67, 155108 (2003).

[30] Hostert, C., Music, D., Bednarcik, J., Keckes, J., Kapaklis, V., Hjörvarsson, B., & Schneider, J.M., *Ab initio* molecular dynamics model for density, elastic properties and short range order of Co-Fe-Ta-B metallic glass thin films. *J. Phys.: Condens. Matter* 23, 475401 (2011).

[31] Hostert, C., Music, D., Kapaklis, V., Hjörvarsson, B., & Schneider, J.M., Density, elastic and magnetic properties of Co–Fe–Ta–Si metallic glasses by theory and experiment. *Scripta Mater.* 66, 765-768 (2012).

[32] Birch, F., Finite Strain Isotherm and Velocities for Single-Crystal and Polycrystalline NaCl at High Pressures and 300°K. *J. Geoph. Res.* 83 (1978).

[33] Holm, B., Ahuja, R., Yourdshadyan, Y., Johansson, B., & Lundqvist, B.I., Elastic and optical properties of *a*- and *k*-Al_2O_3. *Phys. Rev. B* 59, 12777 (1999).

[34] Music, D., Takahashi, T., Vitos, L., Asker, C., Abrikosov, I.A., & Schneider, J.M., Elastic properties of Fe–Mn random alloys studied by *ab initio* calculations. *Appl. Phys. Lett.* 91, 191904 (2007).

[35] Finney, J.L., Random packings and the structue of simple liquids I. The geometry of random close packing. *Proc. Roy. Soc. Lond. A.* 319, 479-493 (1970).

[36] Park, J. & Shibutani, Y., Common erros of applying the Voronoi tesselation technique to metallic glasses. *Intermetallics* 23, 91-95 (2012).

[37] Music, D., Hensling, F., Pazur, P., Bednarcik, J., Hans, M., Schnabel, V., Hostert, C., & Schneider, J.M., Electronic structure and elastic properties of amorphous AlYB14. *Solid State Commun.* 169, 6-9 (2013).

[38] Megusar, J., Low temperature fast-neutron and gamma irradiation of Kapton ® polyimide films. *J. Nucl. Mater.* 245, 185-190 (1997).

[39] Oliver, W.C. & Pharr, G.M., An improved technique for determining hardness and elastic modulus using load displacement sensing indentation experiments. *J. Mater. Res.* 7 (6), 1564-1583 (1992).

[40] Thompson, K., Lawrence, D., Larson, D.J., Olson, J.D., Kelly, T.F., & Gorman, B., In situ site-specific specimen preparation for atom probe tomography. *Ultramicroscopy* 107 (2-3), 131-139 (2007).

[41] Larson, D.J., Prosa, T.J., Ulfig, R.M., Geiser, B.P., & Kelly, T.F., *Local Electrode Atom Probe Tomography*. (Springer New York Heidelberg Dordrecht London, 2013).

[42] Bednarcik, J., Venkataraman, S., Khvostikova, O., Franz, H., Sordelet, D.J., & Eckert, J., Microstructural changes induced by thermal treatment in $Cu_{47}Ti_{33}Zr_{11}Ni_8Si_1$ metallic glass. *Mater. Sci. Eng. A* 498, 335-340 (2008).

[43] Hammersley, A.P., Svensson, S.O., Hanfland, M., Fitch, A.N., & Häusermann, D., TWO-DIMENSIONAL DETECTOR SOFTWARE: FROM REAL DETECTOR TO IDEALISED IMAGE OR TWO-THETA SCAN. *High Pressure Research* 14, 235-248 (1995).

[44] Egami, T. & Billinge, S.J.L., *Underneath the Bragg Peaks: Structural analysis of complex materials*. (Elsevier, Oxford, England, 2003).

[45] Wurster, S., Motz, C., & Pippan, R., Characterization of the fracture toughness of micro-sized tungsten single crystal notched specimens. *Philos. Mag.* 92 (14), 1803-1825 (2012).

[46] Standard test method for measurement of fracture toughness, edited by ASTM (2001), Vol. E 1820-01, pp. 1-46.

[47] Shao, Z., Gopinadhan, M., Kumar, G., Mukherjee, S., Liu, Y., O'Hern, C.S., Schroers, J., & Osuji, C.O., Size-dependent viscosity in the super-cooled liquid state of bulk metallic glass. *Appl. Phys. Lett.* 102, 221901 (2013).

[48] Wang, J., Li, R., Xiao, R., Xu, T., Li, Y., Liu, Z., Huang, L., Hua, N., Li, G., Li, Y., & Zhang, Y., Compressibility and hardness of Co-based bulk metallic glass: A combined experimental and density functional theory study. *Appl. Phys. Lett.* 99, 151911 (2011).

[49] Michalik, S., Gamová, J., Bednarcik, J., & Varga, R., In situ structural investigation of amorphous and nanocrystalline $Fe_{40}Co_{38}Mo_4B_{18}$ microwires. *J. Alloys Compd.* 509, 3409-3412 (2011).

[50] Taghvai, A.H., Stoica, M., Khoshkhoo, M.S., Kaban, I., Bednarcik, J., Jóvári, P., Janghorban, K., & Eckert, J., DSC, XRD and TEM characterization of glassy $Co_{40}Fe_{22}Ta_8B_{30}$ alloy with very high thermal stabalility. *Mater. Lett.* 93, 322-325 (2013).

[51] Waal, B.W.v.d., On the origin of second-peak splitting in the static structure factor of metallic glasses. *J. Non-Cryst. Solids* 189, 118-128 (1995).

[52] Hui, X., Lin, D.Y., Chen, X.H., Wang, W.Y., Wang, Y., Shang, S.L., & Liu, Z.K., Structural mechanism for ultrahigh-strength Co-based metallic glasses. *Scripta Mater.* 68, 257-260 (2013).

[53] Frauenheim, T., Seifert, G., Elstner, M., Niehaus, T., Köhler, C., Amkreutz, M., Sternberg, M., Hajnal, Z., Carlo, A.D., & Suhai, S., Atomistic simulations of complex materials: ground-state and excited-state properties. *J. Phys. Condens. Matter* 14, 3015-3047 (2002).

[54] Qin, J., Gu, T., & Yang, L., Structural and dynamical properties of $Fe_{78}Si_9B_{13}$ alloy during rapid quenching by first principles molecular dynamic simulation. *J. Non-Cryst. Solids* 355, 2333-2338 (2009).

[55] Zhang, L., Cheng, Y., Cao, A., Xu, J., & Ma, E., Bulk metallic glasses with large plasticity: Composition design from the structural perspective. *Acta Mater.* 57, 1154-1164 (2009).

[56] Schuh, C.A., Lund, A.C., & Nieh, T.G., New regime of homogeneous flow in the deformation map of metallic glasses: elevated temperature

nanoindentation experiments and mechanistic modeling. *Acta Mater.* 52, 5879-5891 (2004).

[57] Li, L., Wang, N., & Yan, F., Transient response in metallic glass deformation: A study based on shear transformation zone dynamics simulations. *Scripta Mater.* 80, 25-28 (2014).

[58] Greer, A.L., Cheng, Y.Q., & Ma, E., Shear bands in metallic glasses. *Mater. Sci. Eng., R* 74, 71-132 (2013).

[59] Sin'ko, G.V. & Smirnov, N.A., *Ab initio* calculations of elastic constants and thermodynamic properties of bcc, fcc, and hcp Al crystals under pressure. *J. Phys. Condens. Matter* 14, 6989-7005 (2002).

[60] Gebhardt, T., Music, D., Kossmann, D., Ekholm, M., Abrikosov, I.A., Vitos, L., & Schneider, J.M., Elastic properties of fcc Fe–Mn–X (X = Al, Si) alloys studied by theory and experiment. *Acta Mater.* 59, 3145-3155 (2011).

[61] Wang, H. & Li, M., *Ab initio* calculations of second-, third-, and fourth-order elastic constants for single crystals. *Phys. Rev. B* 79, 224102 (2009).

[62] Fujita, K., Zhang, W., Shen, B., Amiya, K., Ma, C.L., & Nishiyama, N., Fatigue properties in high strength bulk metallic glasses. *Intermetallics* 30, 12-18 (2012).

[63] Madge, S.V., Louzguine-Luzgin, D.V., Lewandowski, J.J., & Greer, A.L., Toughness, extrinsic effects and Poisson's ratio of bulk metallic glasses. *Acta Mater.* (60), 4800-4809 (2012).

[64] Inoue, A., STABILIZATION OF METALLIC SUPERCOOLED LIQUID AND BULK AMORPHOUS ALLOYS. *Acta Mater.* 48, 279-306 (2000).

[65] Albe, K., Ritter, Y., & Sopu, D., Enhancing the plasticity of metallic glasses: Shear band formation, nanocomposites and Nanoglasses investigated by molecular dynamics simulations. *Mech. Mater.* 67, 94-103 (2013).

[66] Schnabel, V., Bednarcik, J., Music, D., Pazur, T., Hostert, C., & Schneider, J.M., Temperature-Induced Short-Range Order Changes in $Co_{67}B_{33}$ Glassy Thin Films and Elastic Limit Implications. *MRL* (2015).

[67] Gu, X.J., Poon, J., Shiflet, G.J., & Widom, M., Mechanical properties, glass transition temperature, and bond enthalpy trends of high metalloid Fe-based bulk metallic glasses. *Appl. Phys. Lett.* 92, 161910 (2008).

[68] Kaban, I., Jovari, P., Waske, A., Stoica, M., Bednarcik, J., Beuneu, B., Mattern, N., & Eckert, J., Atomic structure and magnetic properties of Fe–Nb–B metallic glasses. *J. Alloys Compd.* 586, 189-193 (2014).

[69] Bednarcik, J., Saksl, K., Nicula, R., Roth, S., & Franz, H., Influence of cryomilling on structure of CoFeZrB alloy. *J. Non-Cryst. Solids* 354, 5117-5119 (2008).

[70] Taghvaei, A.H., Stoica, M., Khoshkhoo, M.S., Kaban, I., Bednarcik, J., Jóvári, P., Janghorban, K., & Eckert, J., DSC, XRD and TEM characterization of glassy $Co_{40}Fe_{22}Ta_8B_{30}$ alloy with very high thermal stabalility. *Mater. Lett.* 93, 322-325 (2013).

[71] Chen, N., Martin, L., Luzguine-Luzgin, D.V., & Inoue, A., Role of Alloying Additions in Glass Formation and Properties of Bulk Metallic Glasses. *Materials* 3, 5320-5339 (2010).

[72] Wang, Q., Liu, C.T., Yang, Y., Liu, J.B., Dong, Y.D., & Lu, J., The atomic-scale mechanism for the enhanced glass-forming-ability of a Cu-Zr based bulk metallic glass with minor element additions. *Science* 4, 4648 (2014).

[73] Schnabel, V., Bednarcik, J., Music, D., Pazur, T., Hostert, C., & Schneider, J.M., Temperature-Induced Short-Range Order Changes in $Co_{67}B_{33}$ Glassy Thin Films and Elastic Limit Implications. *Mater. Res. Lett.* 3 (2), 82-87 (2015).

[74] Ding, J., Cheng, Y.-Q., & Ma, E., Full icosahedra dominate local order in Cu64Zr34 metallic glass and supercooled liquid. *Acta Mater.* 69, 343-354 (2014).

[75] Soinila, E., Antin, K., Bossuyt, S., & Hänninen, H., Bulk metallic glass tube casting. *J. Alloys Compd.* 509s, S210-S213 (2011).

[76] Laws, K.J., Gun, G., & Ferry, M., Effect of die-casting parameters on the production of high quality bulk metallic glass samples. *Materials Sci. and Eng. A* 425, 114-120 (2006).

[77] Wu, S., Shen, B., & Inoue, A., Preparation and properties study of bulk $Fe_{75.5}Ga_3P_{10.5}C_4B_4Si_3$ metallic glass ring by copper mold casting. *Intermetallics* 12, 1261-1264 (2004).

[78] Liebermann, H.H. & Graham, C.D., PRODUCTION OF AMORPHOUS ALLOY RIBBONS AND EFFECTS OF APPARATUS PARAMETERS ON RIBBON DIMENSIONS. *Trans. Mag.* 12, 921-923 (1976).

[79] Taghvaei, A.H., Stoica, M., Bednarcik, J., Kaban, I., Shahabi, H.S., Khoshkhoo, M.S., Janghorban, K., & Eckert, J., Influence of ball milling on atomic structure and magnetic properties of $Co_{40}Fe_{22}Ta_8B_{30}$ glassy alloy. *Mater. Charact.* 92, 96-105 (2014).

[80] Shen, B. & Inoue, A., Enhancement of the fracture strength and glass-forming ability of CoFeTaB bulk glassy alloy. *J. Phys. Condens. Matter* 17, 5647-5653 (2005).

[81] Inoue, A., Shen, B.L., & Chang, C.T., Fe- and Co-based bulk glassy alloys with ultrahigh strength. *Intermetallics* 14 (936-944) (2006).

[82] Gebhardt, T., Music, D., Takahashi, T., & Schneider, J.M., Combinatorial thin film materials science: From alloy discovery and optimization to alloy design. *Thin Solid Films* 520, 5491-5499 (2012).

[83] Ding, S., Liu, Y., Li, Y., Liu, Z., Sohn, S., Walker, F.J., & Schroers, J., Combinatorial development of bulk metallic glasses. *Nature Mater.* 13, 494-500 (2014).

[84] Guan, P.F., Fujita, T., Hirata, A., Liu, Y.H., & Chen, M.W., Structural Origins of the Excellent Glass Forming Ability of $Pd_{40}Ni_{40}P_{20}$. *Phys. Rev. Lett.* 108, 175501 (2012).

[85] Yang, W., Liu, H., Zhao, Y., Inoue, A., Jiang, K., Huo, J., Ling, H., Li, Q., & Shen, B., Mechanical properties and structural features of novel Fe-based bulk metallic glasses with unprecedented plasticity. *Sci. Rep.* 4, 6233 (2014).

[86] Liu, Y., Hata, S., Wada, K., & Shimokohbe, A., Thermal, Mechanical and Electrical Properties of Pd-Based Thin-Film Metallic Glass. *Jpn. J. Appl. Phys.* 40, 5382-5388 (2001).

[87] Seah, M.P., Clifford, C.A., Green, F.M., & Gilmore, I.S., An accurate semi-empirical equation for sputtering yields I: for argon ions. *Surf. Interface Anal.* 37, 444-458 (2005).

[88] Cohen, M.L., Calculation of bulk moduli of diamond and zinc-blende solids. *Phys. Rev. B* 32 (12), 7988-7991 (1985).

[89] Moody, M.P., Stephenson, L.T., Ceguerra, A.V., & Ringer, S.P., Quantitative binomial distribution analyses of nanoscale like-solute atom clustering and segregation in atom probe tomography data. *Microsc Res Tech* 71 (7), 542-550 (2008).

[90] Du, X.H., Huang, J.C., Chen, H.M., Chou, H.S., Lai, Y.H., Hsieh, K.C., Jang, J.S.C., & Liaw, P.K., Phase-separated microstructures and shear-banding behavior in a designed Zr-based glass-forming alloy. *Intermetallics* 17 (8), 607-613 (2009).

[91] He, J., Mattern, N., Tan, J., Zhao, J.Z., Kaban, I., Wang, Z., Ratke, L., Kim, D.H., Kim, W.T., & Eckert, J., A bridge from monotectic alloys to liquid-phase-separated bulk metallic glasses: Design, microstructure and phase evolution. *Acta Mater.* 61 (6), 2102-2112 (2013).

[92] Barbee, T.W., Holmes, W.H., Keith, D.L., & Pyzyna, M.K., SYNTHESIS OF AMORPHOUS NIOBIUM-NICKEL ALLOYS BY VAPOR QUENCHING. *Thin Solid Films* 45, 591-599 (1977).

[93] Abdulkadhim, A., to Baden, M., Schnabel, V., Hans, M., Thieme, N., Polzer, C., Polcik, P., & Schneider, J.M., Crystallization kinetics of V_2AlC. *Thin Solid Films* 520, 1930-1933 (2012).

[94] Wang, W.H., The elastic properties, elastic models and elastic perspectives of metallic glasses. *Prog. Mater Sci.* 57 (3), 487-656 (2012).

[95] Park, E.S. & Kim, D.H., Phase separation and enhancement of plasticity in Cu–Zr–Al–Y bulk metallic glasses. *Acta Mater.* 54, 2597-2604 (2006).

[96] Moody, M.P., Stephenson, L.T., Ceguerra, A.V., & Ringer, S.P., Quantitative Binomial Distribution Analyses of Nanoscale Like-Solute Atom Clustering and Segregation in Atom Probe Tomography Data. *Microsc. Res. Tech.* 71, 542-550 (2008).

[97] Lewandowski, J.J., Gu, X.J., Nouri, A.S., Poon, S.J., & Shiflet3, G.J., Tough Fe-based bulk metallic glasses. *Appl. Phys. Lett.* 92, 091918 (2008).

[98] Raghavan, R., Murali, P., & Ramamurty, U., On factors influencing the ductile-to-brittle transition in a bulk metallic glass. *Acta Mater.* 57, 3332-3340 (2009).

[99] He, Q., Cheng, Y.-Q., Ma, E., & Xu, J., Locating bulk metallic glasses with high fracture toughness: Chemical effects and composition optimization. *Acta Mater.* 59, 202-215 (2011).

[100] Schroers, J. & Johnson, W.L., Ductile Bulk Metallic Glass. *Phys. Rev. Lett.* 93, 255506 (2004).

[101] Madge, S.V., Louzguine-Luzgin, D.V., Lewandowski, J.J., & Greer, A.L., Toughness, extrinsic effects and Poisson's ratio of bulk metallic glasses. *Acta Mater.* 60, 4800-4809 (2012).

[102] Pan, D., Inoue, A., Sakurai, T., & Chen, M.W., Experimental characterization of shear transformation zones for plastic flow of bulk metallic glasses. *PNAS* 105, 14769-14772 (2008).

[103] Jang, D., Gross, C.T., & Greer, J.R., Effects of size on the strength and deformation mechanism in Zr-based metallic glasses. *Int. J. Plast.* 27, 858-867 (2011).